2017

PIV Analysis of Wake Structure of Real Elephant Seal Whiskers

Joseph Antun Bunjevac
Cleveland State University

PIV Analysis of Wake Structure of Real Elephant Seal Whiskers

JOSEPH ANTUN BUNJEVAC

BACHELORS OF SCIENCE IN AEROSPACE ENGINEERING

Rochester Institute of Technology

submitted in partial fulfillment of the requirements for the degree

MASTERS OF SCIENCE IN MECHANICAL ENGINEERING

at the

CLEVELAND STATE UNIVERSITY

May 2017

We hereby approve this thesis for

Joseph Antun Bunjevac

Candidate for the Master of Science in Mechanical Engineering degree for the

Department of Mechanical Engineering

and the CLEVELAND STATE UNIVERSITY

and the College of Graduate Studies

Thesis Committee Chairperson, Dr. Wei Zhang

Department/Date

Dr. Mounir Ibrahim

Department/Date

Dr. Thijs Heus

Department/Date

Student's Date of Defense: May 11th, 2017

I'd like to dedicate this to my parents, who not only were successful in convincing me to complete my masters, but supported me through the years of work to complete it.

ACKNOWLEDGMENTS

I would like to acknowledge the following people who have helped me along my way:

NASA Glenn for contributing the whisker specimens used in this study.

Cleveland State for providing the opportunity to perform this research.

Sarah McClure for providing help with learning the PIV system.

Justin Flaherty for assisting in the setup and running of much of the testing and data collection presented in this paper.

Aidan Rinehart for providing assistance in testing and in writing of this Thesis.

Dr. Wei Zhang for providing constant guidance and pushing for high standards for the work presented here.

PIV Analysis of Wake Structure of Real Elephant Seal Whiskers

JOSEPH ANTUN BUNJEVAC

ABSTRACT

Seals are able to accurately detect minute disturbances in the ambient flow environment using their whiskers, which is attributed to the exceptional capability of their whiskers to suppress vortex-induced vibrations in the wake. To explore potential applications for designing smart flow devices, such as high-sensitivity underwater flow sensors and drag reduction components, researchers have studied how the role of some key parameters of whisker-like morphology affect the wake structure. Due to the naturally presented variation in size and curvature along the length of whiskers, it is not well understood how a real whisker changes the surrounding flow and the vortex shedding behavior. This study aims to detail the flow statistics around a real Elephant Seal whisker at low Reynolds numbers (i.e. one hundred) using particle image velocimetry in a water channel. Wake flow structures are inspected and compared between two Elephant Seal whiskers (undulating) and a California Sea Lion whisker (smooth), along with idealized whisker-like models. Undulating whiskers significantly change the mean flow properties and suppress turbulence intensities in the wake region as compared to the smooth whisker at the tested Re. The undulating whiskers are able to create a low turbulence intensity area directly behind the whiskers trailing,

providing these whiskers with their Vortex Induced Vibration reduction properties.

TABLE OF CONTENTS

LIST OF TABLES

LIST OF FIGURES

CHAPTER I

Introduction

1.1 Background Information

Whiskers are a feature found on many different animals used for sensing their surrounding environment. Whiskers (also known as vibrissae) can be used to sense the environment through haptic sensing [19], or through flow sensing. Seals use their whiskers to detect flow fluctuations or flow conditions as they swim through the water. The higher the sensitivity of the whiskers, the greater the chance for the seal to track and catch prey. Seals which live in areas with reduced visibility have had to evolve their whiskers for amplified sensitivity. The typical whisker is a constant cylindrical shape which reduces in diameter along the main axis to the tip. Some species of seals, such as the Elephant Seal, have a unique undulating morphology of elliptical-shaped cross-sections. This geometry shows superior performance with regard to vortex induced vibration reduction and flow sensitivity and has been a source of interest and study as early as 1977 [8] [7] [6].

A study by Hanke [1] clearly demonstrated the level of sensitivity of seal species

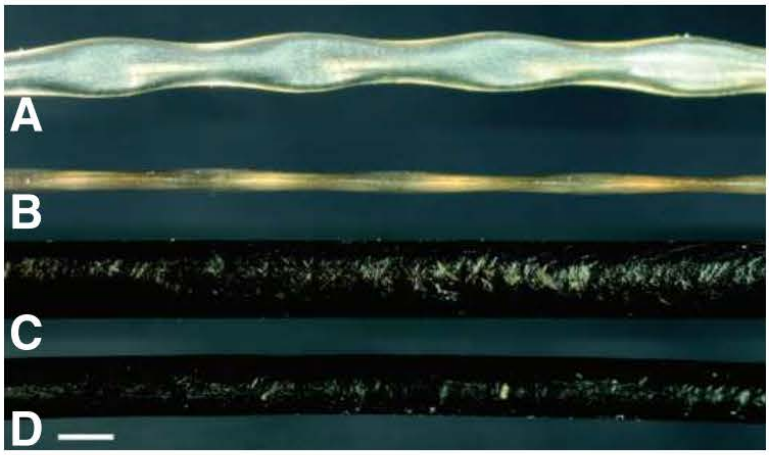

Figure 1: Two plane view of: A and B - Harbor Seal Whisker, C and D - California Sea Lion Whisker [1]

with undulating whiskers. In his experiment, a Harbor seal was blindfolded in a water tank with a wake creating device that the seal was tasked with tracking. The experiment showed that the seal was able to detect flow fluctuations as small as 0.25 mm/s. A CCD camera recorded footage of the whiskers to measure the vibration of the whisker during the tracking experiment. Studying the footage revealed that the whisker was not found to vibrate at all, suggesting that if any vibrations occurred, they were less than 0.2mm, which was the resolution limit of the camera sensor. Measurements of the vibration of undulating whiskers have been studied using alternative methods [16]. However, if the vibrissae were obstructed, the seals were not able to track wakes as easily [9] [10].

Figure 2: Experimental setup of wake tracking by blindfolded seal. Camera for observing whisker vibration indicated in red [1]

1.2 Previous Studies on Wake Properties of Undulating Shapes

As a fluid flows around blunt shaped bodies, the object creates alternating vortexes in a phenomenon known as von karman vortex shedding. This vortex shedding induces a force on the object, which may cause vortex induced vibration (VIV). If a whisker is optimally shaped to reduce VIV, the signal to noise ratio for the receptors is increased, and the seal will have a greater ability at sensing the wake of prey fish.

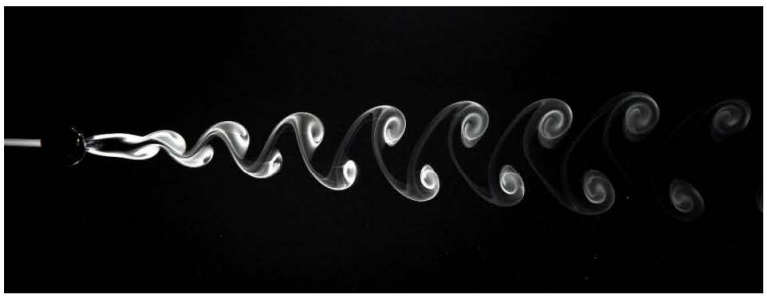

Figure 3: Visualization of a vortex street past a cylinder [21]

One of the critical features of the seal whiskers is the multi-plane undulations. A study performed by Zhang [4] showed that undulations can change the wake structures of objects with circular cross sections. The wavy cylinder created streamwise vorticity streaks of alternating directions which were not present with the smooth cylinder. The results from Jung and Yoon [3] study of wavy cylinders and twisted ellipse showed additional benefits with a decrease in the coefficient of drag and a major decrease in the coefficient of lift fluctuations, which is attributed to the reduction of the von karman vortex shedding. A study on undulating whisker geometry has shown that undulations in both the major and minor axis are necessary for the distruption of von karman vortex shedding [11].

Other studies have focused on the applications of undulating shapes in different flow related areas. Many research studies have focused on the frequency response of undulating whiskers under different conditions [13]. With knowledge of the response of the whisker to different flow conditions, flow sensors can be developed based on the undulating whisker geometry [12]. The flow sensing is dependend on the reaction from the whiskers to the sensing mechanisms, as the whiskers do not contain any nervous sensing devices [20]. Modifications to aerofoils for different applications may also see benefits of undulating geometries [15].

Lin et al [2] provided insight on the function of the undulations as shown in Figure 5. As the fluid flows across the undulating object, the fluid flows from the

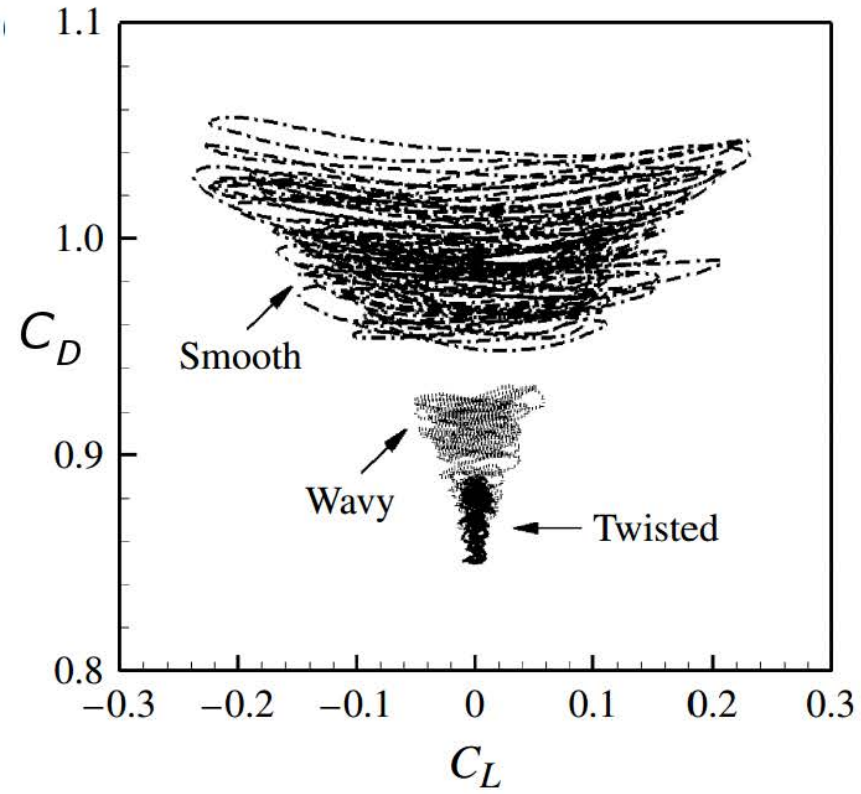

Figure 4: Comparison of the drag coefficient and lift coefficient between a smooth cylinder, a wavy cylinder and a twisted ellipse [3]

peaks to the troughs along the object. The flow then collides and pushes outward, resulting in flow circulation of equal and opposite strength and direction. The wavelength and amplitude ratio of the undulation has a noticeable effect on the shape and strength of these vortices pairs. These vortices are of relatively high strength. After the whisker trailing edge, the vortices combine, mix, and dissipate out.

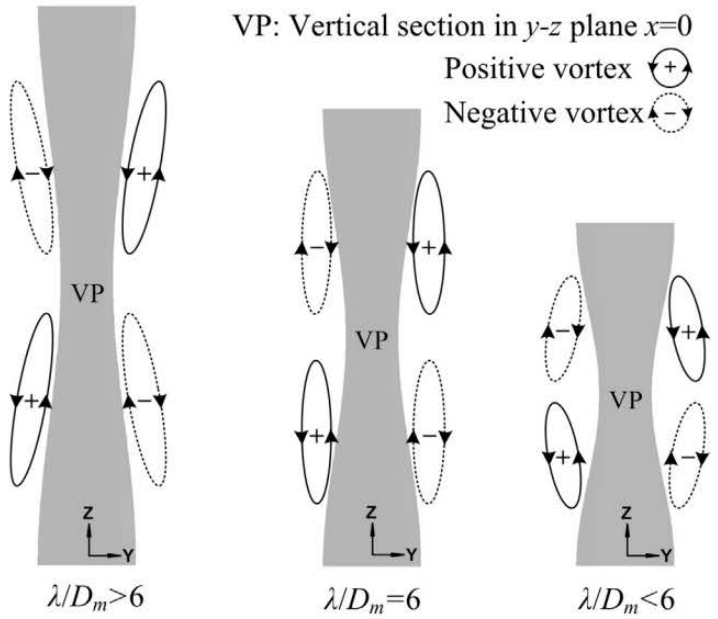

Figure 5: Depiction of shape and direction of rotating vortices induced by wavy surfaces, with different λ/D_m [2]

1.3 Geometric Properties of Undulating Whiskers

The exact shape of undulating whiskers are random enough that no two whiskers are exactly alike, even on the same mammal, but are statistically similar enough that the whiskers can be used to determine the specific species of seals [6]. The simplest description for these undulating whiskers is an elliptical cross-section which varies in both major and minor axis as it moves along the major axis of the whisker. The plane of the ellipse can also tilt in relation to the major axis of the whisker. This tilt or angle causes the wavelength of the undulations to constantly vary.

Hanke introduced a set of seven parameters [1] shown in Figure 6, which describe the geometry of a whisker at each peak and trough location. M defines the half wavelength between adjacent peaks and troughs. The major and minor axis for the peak ellipse are a and b. The trough ellipse geometry is defined by k and l for the major and minor axis. The peak and trough angle of incidences are only defined in the plane parallel with the major axis for the peak and trough. The angle for the

peak to peak plane is defined as α. The angle for the trough to trough angle is β.

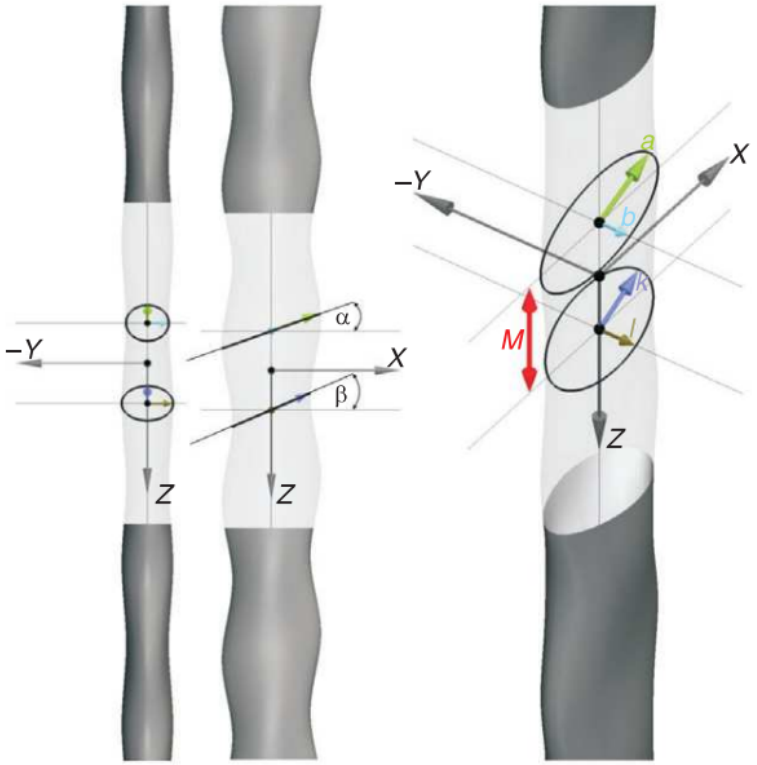

Figure 6: Seven parameters used to define whisker geometry at peaks and troughs [1]

Multiple studies have included measuring the whisker morphology [17] [13]. Rinehart [5] performed a CT scan of 27 harbor seal and elephant seal whiskers to study these seven parameters. For elephant seal whiskers, the half wavelength M was near 2mm. The major axis for the peaks and troughs were 1.223mm and 1.099mm. The ratio of major to minor axis for the peak was 2.11, while the ratio for the trough was 1.71. The angle of incidence for α and β roughly follows a Gaussian distribution shown in figure 7 with a majority of the angle of occurrences ranging between $-10°$ and $10°$.

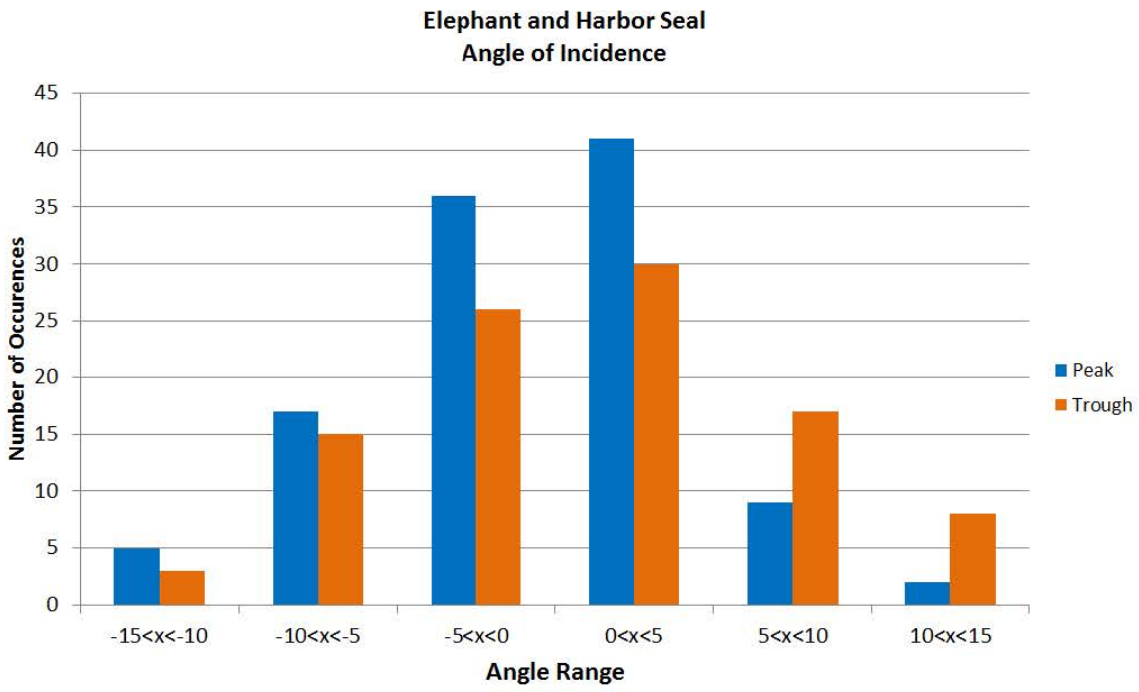

Figure 7: Histogram of the angle of incidence (α and β) of 27 Harbor Seal and Elephant Seal whiskers using CT scanning data [5]

1.4 Study Outline

The goal of this study is to characterize the wake flow around real seal whiskers at low Reynolds numbers and determine flow characteristics which may provide insight to the VIV reduction properties of undulating whiskers. Previous studies have studied the wake produced by scaled models or in CFD simulations [4] [5] [2] [14] [1] [18]. This research will evaluate the flow over two real undulating Elephant Seal whiskers along with a smooth cylindrical California Sea Lion whisker, which were made available to us through collaboration with NASA Glen. Previous studies had a very small field of view, covering only 5 -15 diameters downstream of the whiskers. This flow analysis will cover a large field of view of 30-70 diameters to ensure that the complete flow structure is captured. The research will provide insight into the real affects of the random values for the geometry parameters, importantly the α and β angles, on the wake flow of real whiskers. Previous scaled and simulated studies used fixed values

for the seven whisker geometry parameters. Hanke [1] used values of 15.27° for α and 17.60° for β after averaging the values for 13 different undulating whiskers. Rinehart [5] measured 27 different undulating whiskers and arrived at different averages for angle of incidences. Studies with fixed values may provide insight into methods of shaping the wake flow.

The first section of the study will focus on comparisons between a cylindrical object, represented by the California Sea Lion whisker, and the undulating whiskers. The wake of the whisker are studied in the 2D streamwise vertical and horizontal planes. The second section will focus on the differences between the wakes of peak locations and trough locations. These results will then be compared to the results from a previous study. Finally, a closer examination is performed on the flow features which provide the supression of the vortex induced vibration.

CHAPTER II

Experimental Setup

2.1 Water Channel

The experiment was performed in a constant velocity water channel. The water channel is made of plexiglass with an upper level for flow testing, and a water return below. The channel is 5.5 inches wide. Water is pumped at a constant rate from a reservoir into the top level of the channel. The water travels through the flow conditioners, which consists of six one inch thick aluminum honeycomb sheets, each spaced one inch apart, providing a mean turbulence intensity of 3.5 %. The test section begins 8 inches from the flow conditioners and is 12 inches long. Downstream of the test section is the orific, which controls the water channel level and mean velocity. The orifice plate used provided 8 inches of vertical height and a mean flow velocity of 0.12 m/s. Water is then returned to the reservoir through the channel below the test section, where it is filtered through a 50 micron particle filter.

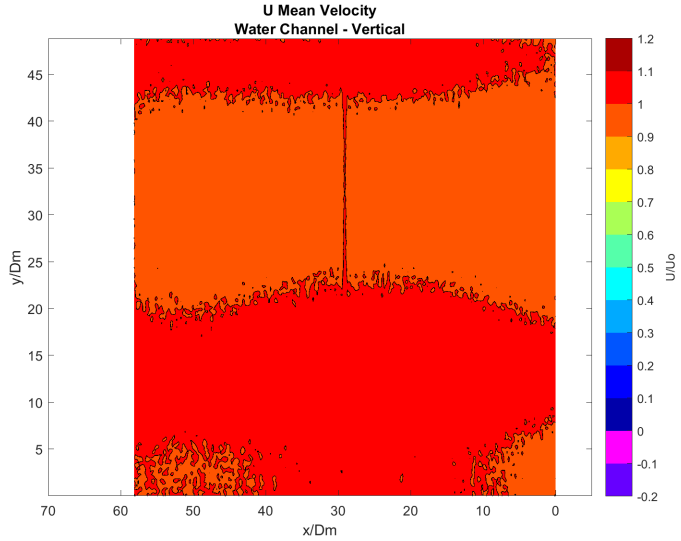

Figure 8: Mean streamwise velocity contours in the vertical center plane of the clean water channel (without whiskers)

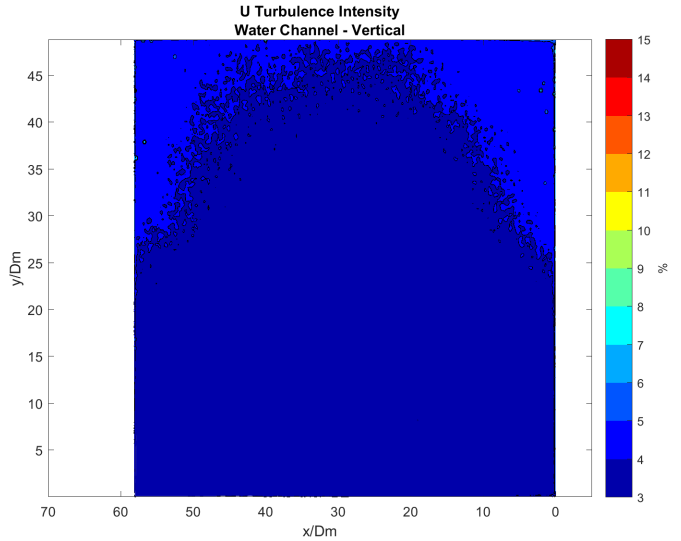

Figure 9: Streamwise turbulence intensity contours in the vertical center plane of the clean water channel (without whiskers)

2.2 PIV System

Data is collected using a LaVision 2D PIV system. PIV (Particle Image Velocimetry) is a flow analysis method which uses light and cameras to non-intrusively measure flow velocity. The fluid is seeded with small, neutrally buoyant particles. A laser light sheet illuminates these particles while a camera takes an image. A second image is taken at a known time difference from the first image. This forms an image pair. Software analyzes the image pair to track the distance that each illuminated particle traveled. The particled are grouped into a grid of interrogation windows of a specified size. The particles in the interrogation windows are cross-correlated between the image pairs to determine the displacement for the window. Combined with the known time step, the velocity is determined for each interrogation window, and the flow field for the full image can be processed.

The laser lightsheet is provided by an Evergreen dual-pulsed ND:Yag laser creating a 532nm wavelength beam operating at a maximum speed of 14.7Hz and 200mJ energy output. Images are captured with a LaVision Pro-Imager SX 5MP CCD camera fitted with a Nikon AF Micro-Nikkor 60mm f/2.8D lense and a 532 + 5nm light wavelength filter. The water channel is seeded with coated glass spheres 10 m in diameter. The laser and camera are controlled by DaVis LaVision software package version 8.2.

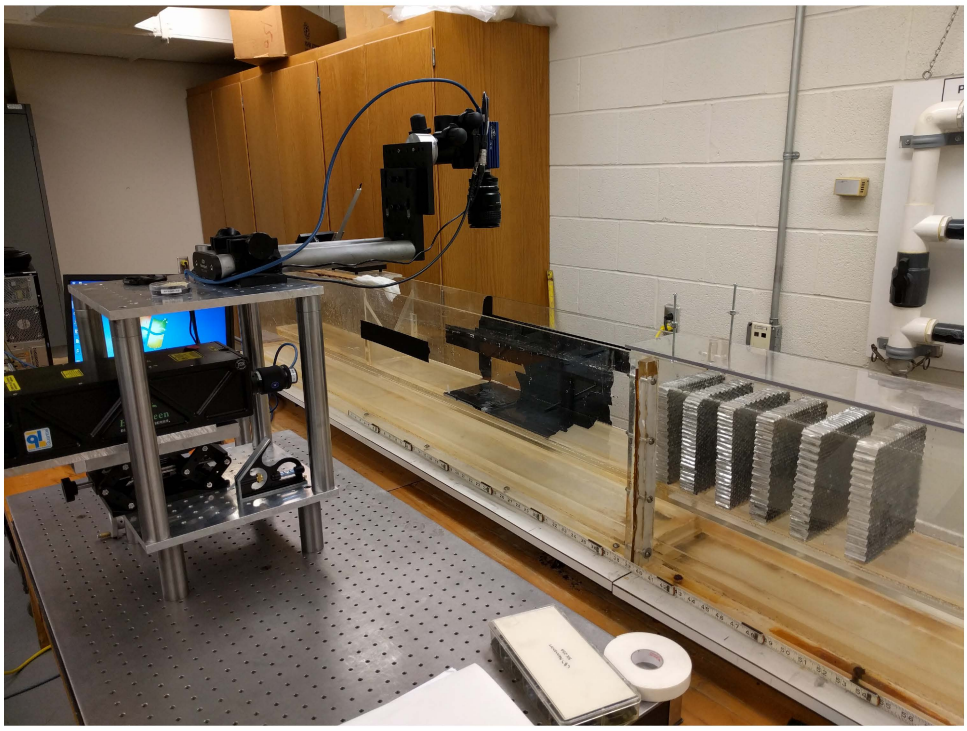

Figure 10: PIV experiment setup for the horizontal plane measurements

2.3 Whisker Setup

The whiskers were mounted on 1/16 in diameter shafts using non-reflective black tape. The shaft was placed in an oversized shaft clamp, which was filled with modeling clay. The clay provided sufficient flexibility to adjust the whisker in a vertical orientation while holding firmly enough to not move during the experiment. The shaft clamp is placed in a matching diameter hole in a 6in x 5.5in x 0.25in aluminum plate. The plate is a snug fit in the inside of the water channel, which ensures the whisker is positioned in the center of the water channel, reducing the wall effects on the data. The baseplate is covered in non-reflective black tape, leaving a small opening for the shaft, to minimuze light reflections.

The orientation of the whiskers was important when placing them in the channel. The desired test area is required to be as vertical as possible, with a 0° angle of attack with the flow. Any tilt in the whisker or rotation in the angle of attack will

create a significantly different wake flow. Real whiskers are not perfectly straight or planar. They have a natural backwards curve as well as arbitrarily bending sideways. This real geometry provided challenges with the laser light sheet alignment. The whisker mount shafts can easily be twisted to obtain the 0° angle of attack. Due to the small diameter of the upper region of the whisker, the lightsheet was positioned at the lower 2/3 of the whisker to avoid alignment difficulties. The whisker mount was tilted to position the lower section of the whisker in a vertical orientation. For the vertical plane, the lightsheet was positioned to align with the maximum possible area of the whisker. Reviewing the resulting data would clearly show if the light sheet was correctly positioned on the center of the whisker. It was unavoidable to have the whiskers bend in and out of the light sheet, and this entering and exiting of the light sheet is visible in the data.

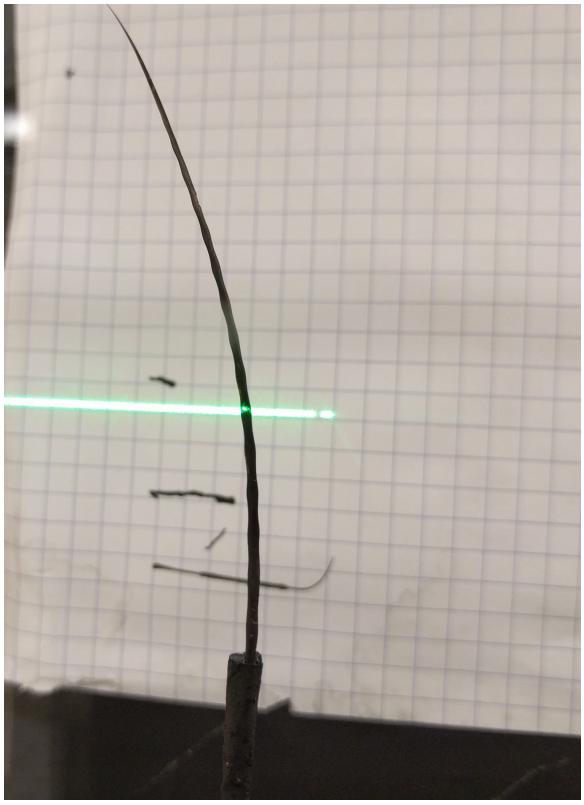

Figure 11: Independent image to identify the location of the light sheet with respect to the real-scale whisker.

Two equipment setups were used to obtain the vertical and horizontal data planes. The vertical plane is positioned at the whisker centerline to capture the full streamwise and vertical flow qualities. For the undulating whiskers, three pairs of horizontal planes are taken at different distances from the root of the whisker. One horizontal plane is at a peak location, and the other is at an adjacent trough location. This allows comparison of flow qualities at the peaks and troughs to be compared, as the elliptical geometry varies significantly. Multiple locations along the main axis allowed comparison between different hydraulic diameters and Reynolds numbers.

Linear actuators allowed controlled placement of the laser sheet at the desired locations. A Velmex UniSlide A40 linear actuator with a 0.025in / rev lead screw allowed precise positioning of the vertical light sheet. Due to the sideways curving of the undulating whiskers, careful consideration was required to minimize the area the whisker curved out of the light sheet. This was done using careful visual verification and observing the live view images of the PIV camera system. A ThorLabs L490 Lab Jack provided the positional control for the horizontal light sheet position. Horizontal plane positions could be verified using a second consumer camera with a contrasting background as shown in Figure 11.

Three whiskers were tested in total: Two Elephant Seal whiskers, noted as Whisker A and Whisker B, and one California Sea Lion whisker, noted as Smooth Whisker. These whiskers were provided in collaboration by NASA Glen who is performing related studies with whiskers. The geometry of the whiskers used is measured and tabulated in Table I. The geometry of the whiskers is compared to the CT Scan data from Rinehart in Table II. While α and β values are not able to be compared, the elliptical geometry of the peaks and troughs are within the standard deviations.

Table I: Summary of geometry parameters and the Reynolds numbers (based on the hydraulic diameter and mean inflow flow velocity) for three whiskers

Whisker	**Plane**	**Root Location**	**a (mm)**	**b (mm)**	**k (mm)**	**l (mm)**	**Dh (mm)**	**Re**
Whisker B	Horizontal	Base	1.151	0.576	—	—	0.728	87
Whisker B	Horizontal	Base	—	—	1.058	0.705	0.830	99
Whisker B	Horizontal	Middle	0.934	0.467	—	—	0.591	71
Whisker B	Horizontal	Middle	—	—	0.745	0.497	0.584	70
Whisker B	Horizontal	Top	0.846	0.423	—	—	0.535	64
Whisker B	Horizontal	Top	—	—	0.658	0.439	0.516	62
Whisker A	Horizontal	Base	1.273	0.637	—	—	0.805	96
Whisker A	Horizontal	Base	—	—	1.024	0.683	0.803	96
Whisker A	Horizontal	Middle	1.183	0.592	—	—	0.748	89
Whisker A	Horizontal	Middle	—	—	0.934	0.623	0.733	88
Whisker A	Horizontal	Top	0.913	0.457	—	—	0.577	69
Whisker A	Horizontal	Top	—	—	0.785	0.523	0.616	74
Smooth Whisker	Horizontal	Base	1.307	1.307	1.307	1.307	0.934	112
Smooth Whisker	Horizontal	Middle	1.18	1.18	1.18	1.18	1.180	141
Smooth Whisker	Horizontal	Top	0.934	0.934	0.934	0.934	1.307	156
Smooth Whisker	Vertical	—	1.121	1.121	1.121	1.121	1.121	134
Whisker B	Vertical	—	0.999	0.500	0.999	0.500	0.632	76
Whisker A	Vertical	—	1.093	0.547	1.093	0.547	0.691	83

Table II: Key geometry parameters measured from PIV images, compared with statistical data from CT scanning [5]

	Elephant Seal	α **(Deg)**	**a (mm)**	**b (mm)**	**M (mm)**
Rinehart	Mean	-0.400	1.233	0.583	1.957
	Std Dev	4.248	0.386	0.214	0.375
Bunjevac	Mean	—	1.050	0.525	—
	Std Dev	—	0.174	0.087	—
	Elephant Seal	β **(Deg)**	**k (mm)**	**l (mm)**	**Dh (mm)**
Rinehart	Mean	-1.088	1.099	0.642	0.890
	Std Dev	9.139	0.414	0.248	0.267
Bunjevac	Mean	—	0.867	0.578	0.672
	Std Dev	—	0.162	0.108	0.114

2.4 Data Processing

The hydraulic diameter is used for Reynolds number calculation and plot scaling. The plots for the horizontal planes used the hydraulic diameter for the local position on the whisker. The vertical plane plots use an averaged estimated diameter for the region studied. Due to the fixed velocity of the water channel, the Reynolds numbers are not matched between test. The Reynolds numbers for these experiments ranged from 62-156, which is based on the changing hydraulic diameters and the fixed water channel velocity. The whisker dimensions were verified using hand measurements and verified using the image data. The raw data from DaVis was kept at units of pixels for dispacement. Once a light sheet setup was finalized, an image of a steel rule positioned level with the light sheet was recorded. The DaVis software tools allowed the user to obtain a relation between the distance in pixels to the distances marked on the steel rule. This pixel to centimeter ratio is used to scale the velocities from pixels per second to meters per second. Using an image of the whisker allows a similar conversion. The shape of the whisker is measured in pixels from a single image at the desired location. The pixel to centimeter ratio is applied to obtain dimensions of the whisker which can be verified against the measurements taken with calipers.

The hydraulic diameter D_h is calculated from the area equation A and the circumference equation P for an ellipse. The circumference equation used in this study is the Euler approximation.

$$A = a \cdot b \cdot \frac{\pi}{4} \tag{2.1}$$

$$P = 2 \cdot \pi \sqrt{(\frac{a^2}{2}) + (\frac{b^2}{2})} \tag{2.2}$$

$$D_h = \frac{(4 \cdot A)}{P} \tag{2.3}$$

Matlab is used to calculate the parameters of interest using the vector data produced by the DaVis LaVision software. This paper provides results for Mean Velocity, Vorticity, Reynolds Shear Stress, TKE, and Streamwise Turbulence Intensity, which will provide information on the mean wake flow structure and the wake turbulence. The plots presented in this paper are the results of performing an ensemble average of the 1200 image pairs. Each of the 1200 vector data points is averaged to obtain the mean velocity field. From this mean value, the individual fluctuation values are calculated for all 1200 points and used to obtain the Urms and Vrms values. The Reynolds stress, Turbulent Kinetic Energy, and Streamwise Turbulence Intensity are calculated from these velocity fluctuations using the following formulas:

$$U_{rms} = \sqrt{\bar{u_i^2}} \tag{2.4}$$

$$\overrightarrow{\omega} = \nabla \times \overrightarrow{u}_{ijk} \tag{2.5}$$

$$\tau_R = \overline{u'v'} \tag{2.6}$$

$$TKE = 0.5 \cdot \rho \left[(\bar{u'})^2 + (\bar{v'})^2 \right] \tag{2.7}$$

$$T_u = \frac{U_{rms}}{U} \tag{2.8}$$

A multi-size interrogation window is used to to analyze the image pairs in DaVis software. A two-pass interrogation size of 32pix x 32pix with 50 % overlap is followed by a second two-pass interrogation of 16pix x 16pix with 50 % overlap. Geometry masking was performed by hand to include the whisker and other artifacts,

including shadows and mounts. The vector post processing included removal of windows with fewer than 4 vectors and removal of vectors which exceeded 2 standard deviations of the neighboring vectors.

CHAPTER III

Flow Statistics and Wake Structures

The following results compare the wake structure of the undulating Elephant Seal whiskers to the smooth Sea Lion whisker against different flow properties. The flow direction and coordinate system is given by Figure 12b. The flow enters from the right and flows to the left in the X axis. The whisker main axis is defined as the Y axis. Each of the graphs contains a white masking of the whisker location. The Elephant Seal whisker plots have horizontal lines which represent the location of the peaks. These horizontal lines do not represent the α or β angle of the whisker geometry, as those angles could not be reliably determined from the raw images. The reynolds numbers do not exactly match between each test case due to the limitation of the fixed water channel velocity.

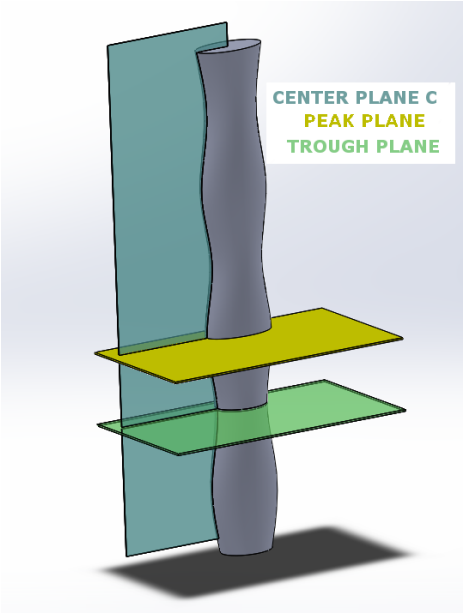

(a)

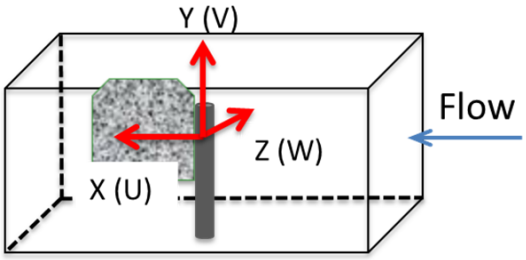

(b)

Figure 12: Coordinate system and light sheet planes used for presenting wake structure and turbulent statistics

3.1 Flow Statistics of the Wake Behind Smooth Whiskers vs Undulating Whiskers

3.1.1 Vertical Plane

For the streamwise mean velocity behind the smooth whisker , we can easily observe the reverse flow near the whisker in Figure 13a, followed by the steady flow recovery afterwards. The shape of the recovery is nicely parallel with the main axis of the whisker. The flow recovery to 50 % of the mean flow is consistent along the main axis of the whisker, with recovery after this level sporadic. The reverse flow region extends to 3-5 diameters, and full recovery nearly achieved by 10 diameters. Some of the erratic downstream flow may be due to the rough surface of the smooth whisker.

The undulating whisker case generated a very structured wake flow for the

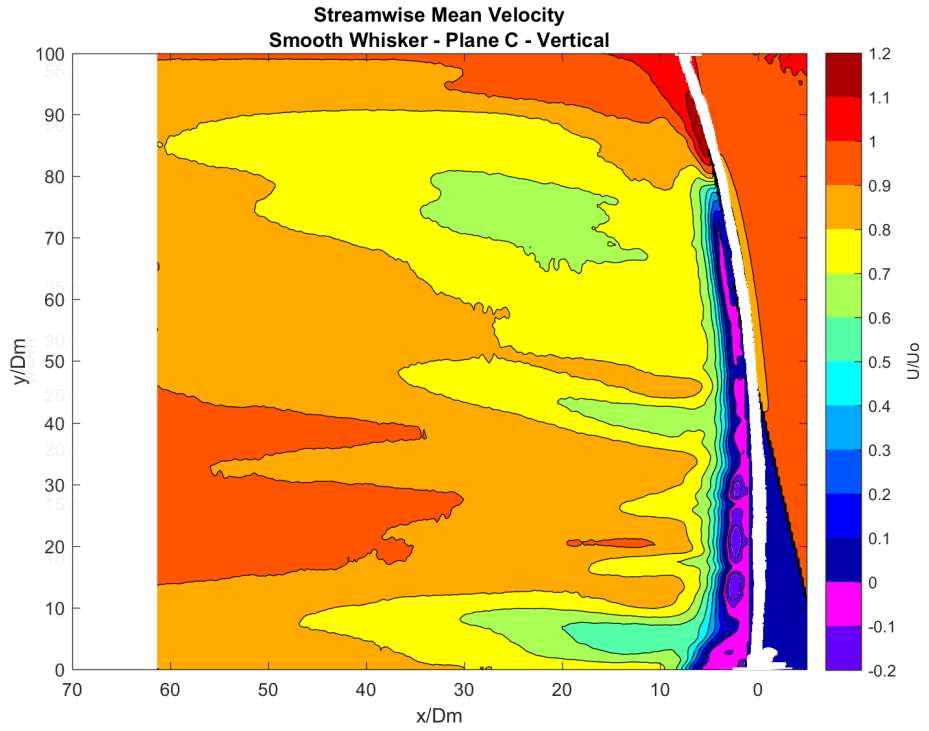

(a) Re = 134

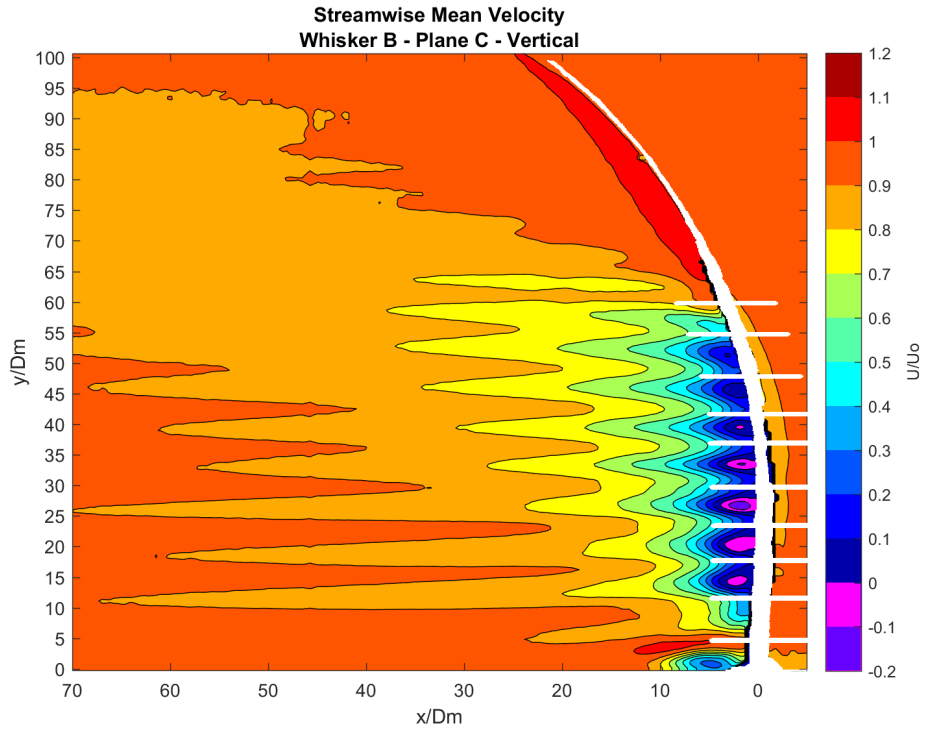

(b) Re = 76

Figure 13: Comparison of the streamwise mean velocity in the wake between the Smooth Whisker and Whisker B in the vertical plane

streamwise mean velocity in Figure 13b. There are small sections of reverse flow located neatly between the whisker peaks about 1-3 diameters long. The faster recovering sections coincide with the peak locations and contain minimal reverse flow. Higher along the whisker, the flow takes longer to fully recover, which is due to the curving of the whisker. The flow recovers to 50 % evenly along the main axis, although it is slower than the smooth whisker case. The tilt in the upper region of the undulating whisker doe not appear to affect the flow recovery before 50 %, but is seen to slow the recovery after this level. Compared to the smooth whisker case, the undulating whisker takes about twice as long to recover to 50 % of the mean flow but is much less erratic in recovering fully with the mean flow. Neither case is clearly significantly faster in recovery to the mean flow.

The vertical mean velocity flow is very erratic for the smooth whisker case shown in Figure 14a. The wake flow at the bottom of the whisker has a strong upwards and downwards flow region, which is most likely a result of the whisker mount interfering with the flow at that lower area. Moving up the whisker's main axis, a section of alternating positive and negative is shown, before turning into a highly positive flow region at the upper section of the whisker. Similar streaky areas are seen in the streamwise mean flow as in the vertical mean flow direction.

The wake in Whisker B shows a moderately structured flow for the V mean direction in Figure 14b. The lower half of the whiskers are dominated by a negative flow, while the upper region is mostly positive flow. Some streaks are visible similar to the waviness in the streamwise mean flow.

Moving to the vorticity plots, we see a significant difference in the structure and uniformity of the wake flow of the two whiskers in Figures 15a and 15b. The smooth whisker case shows a highly varying and highly scattered vorticity. The highest strength vortices are short and very close to the whisker, typically less than

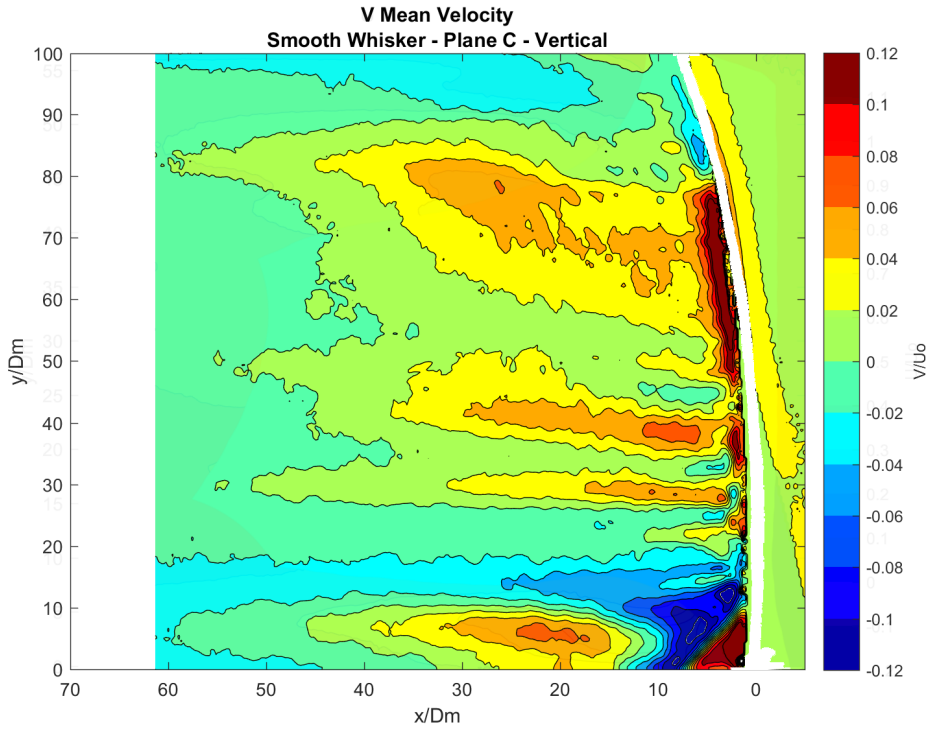

(a) Re = 134

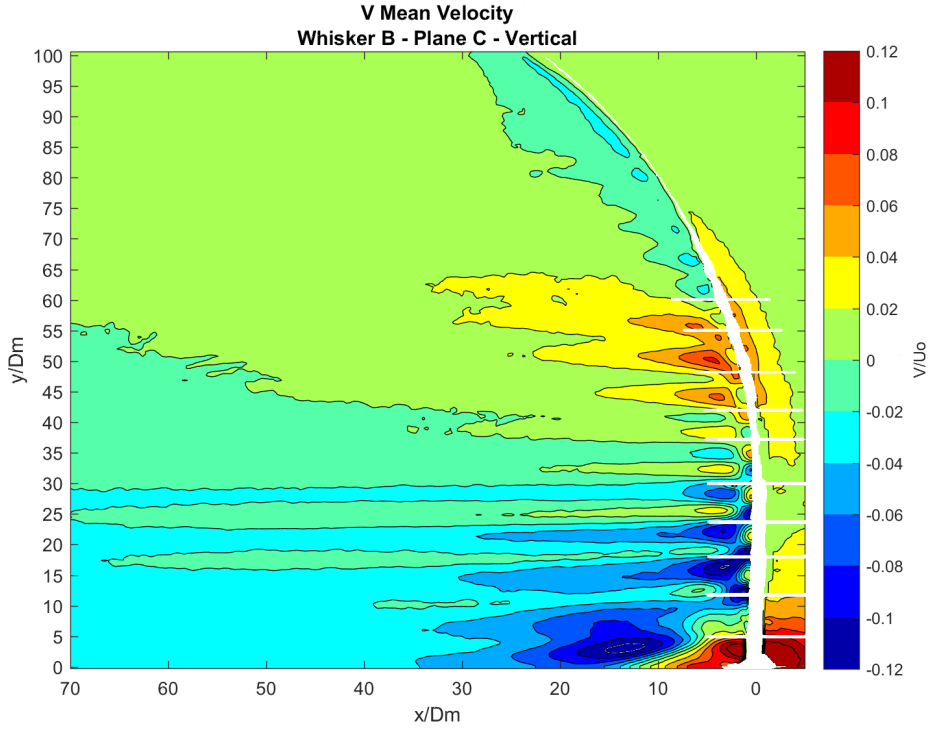

(b) Re = 76

Figure 14: Comparison of the mean vertical velocity in the wake of the undulating and smooth whiskers in the vertical plane

3 diameters. Moderately strong vortices extend out to 20 diameters, and by 30 diameters, the majority of the vortex structures are reduced to very weak levels. The undulating whisker case is much more structured and consistent, with the flow structure extending horizontally with the flow direction. A larger region of high strength vorticity exists up to 10 diameters, which rapidly weakens by 15 diameters and continue far downstream. The mixing as described by Lin2 can clearly be seen in this plot. Positive and negative vortices are paired together between sets of peaks of similar strengths and shapes.

The smooth whisker case produces high levels of Reynolds Shear stress which continue significantly longer than the undulating whisker case as shown in Figure 16. The smooth whisker case has higher values of shear stress up to 30 diameters downstream, with the values predominantly negative. High strength areas are found along the full length of the smooth whisker. The undulating whisker case has longer areas of high levels near the whisker at the base and top locations, but the flow returns to normal levels after 10 diameters downstream. There are nearly equal amounts of positive and negative shear areas, which was not seen in the smooth whisker.

Significant differences are seen in the Turbulence Kinetic Energy wake flows as shown in Figure 17. The smooth whisker case shows high energy values immediately behind the whisker, followed by a large 20 diameter section of moderate energy levels. Recovery to low levels begins to occur 45 diameters downstream. The undulating whisker case shows longer strong areas immediately behind the whisker, followed by a quick reduction in energy. At 15 diameters, the energy level is down to nominal values.

The significant advantage of the undulating whisker's geometry over the smooth cylindrical whisker can be seen in the turbulence wake flow shown in Figure 18. The smooth whisker case has a significantly larger area of high turbulence intensity, which

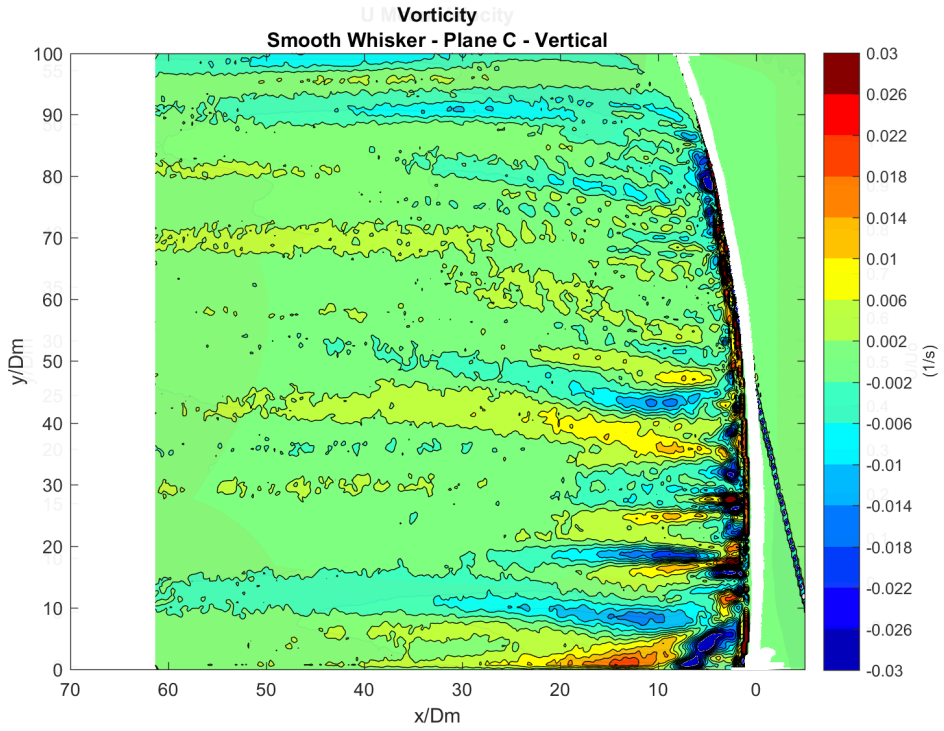

(a) Re = 143

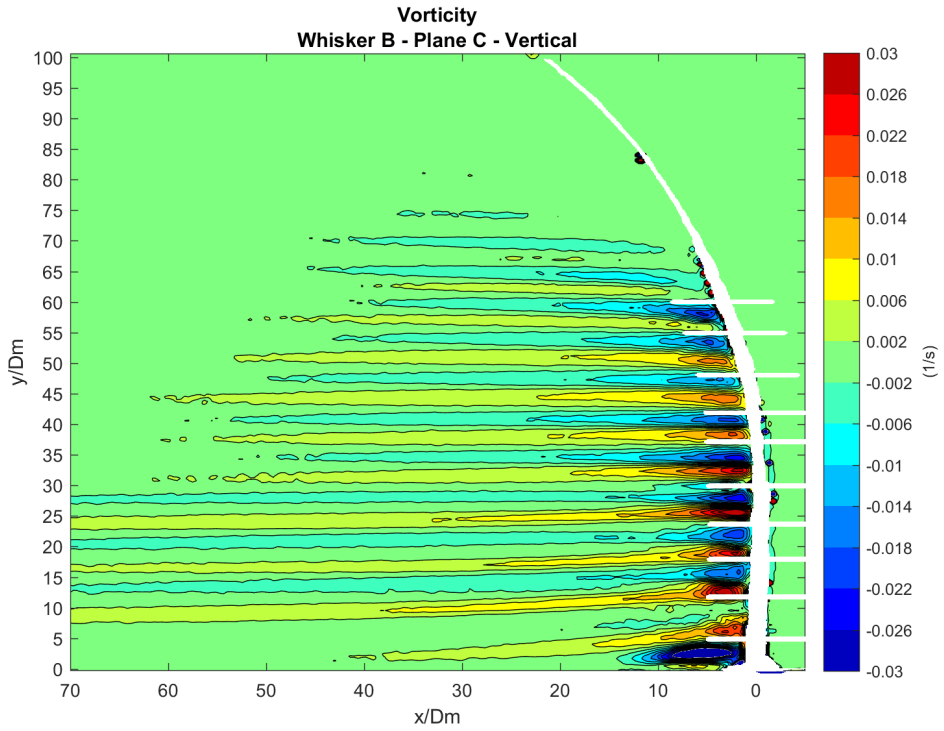

(b) Re = 76

Figure 15: Comparison of the spanwise vorticity ω_z in the wake of the undulating and smooth whiskers in the vertical plane

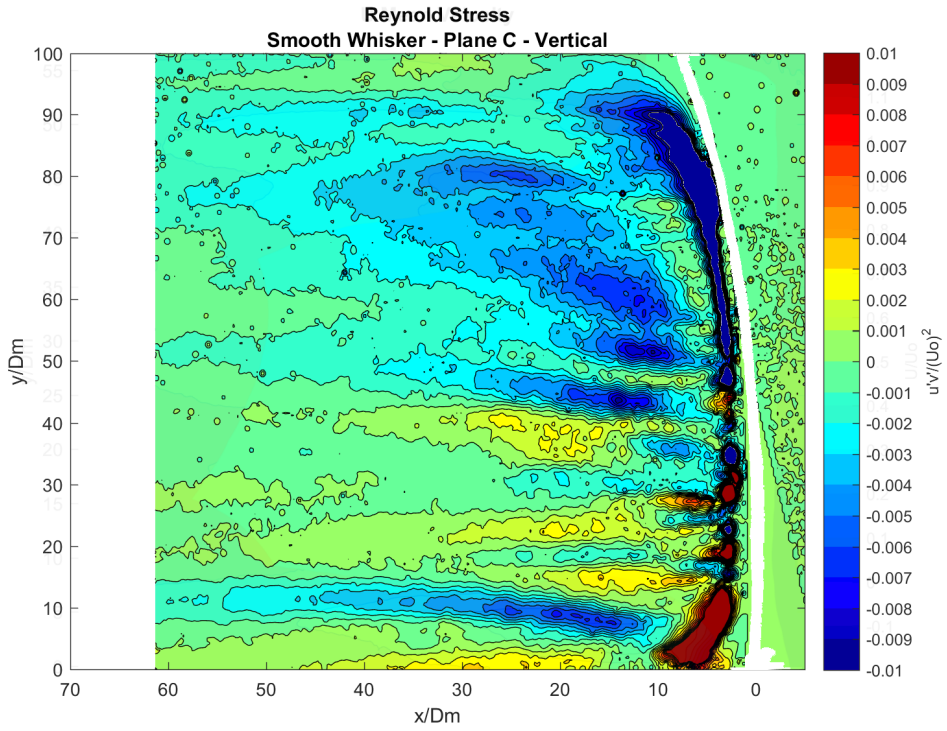

(a) Re = 134

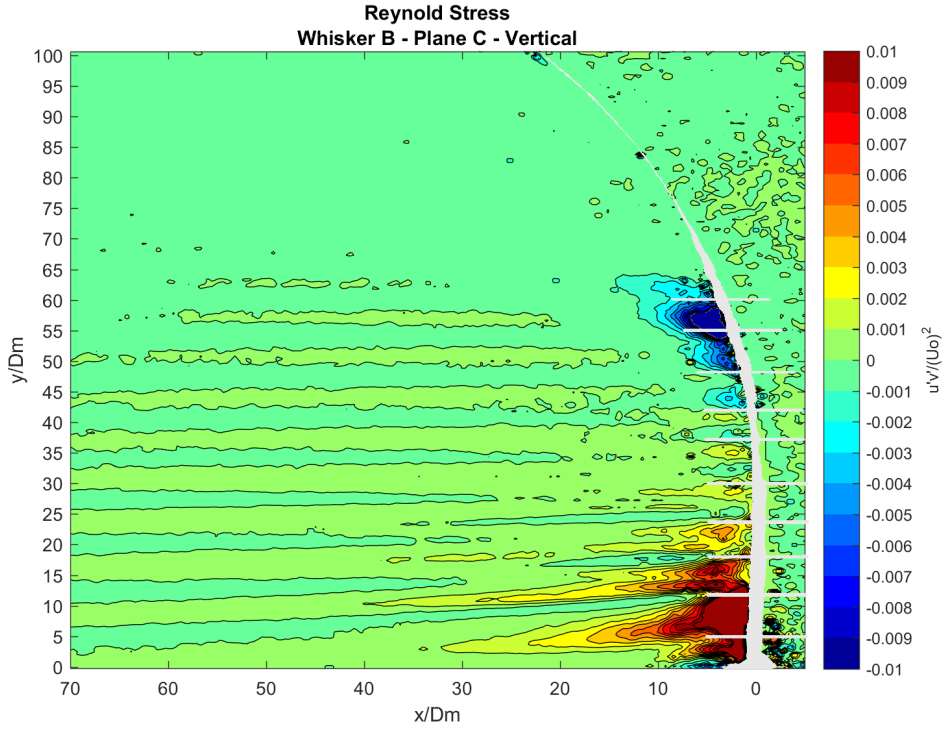

(b) Re = 76

Figure 16: Comparison of the Reynold Stress in the wake of the Smooth Whisker and Whisker B in the vertical plane

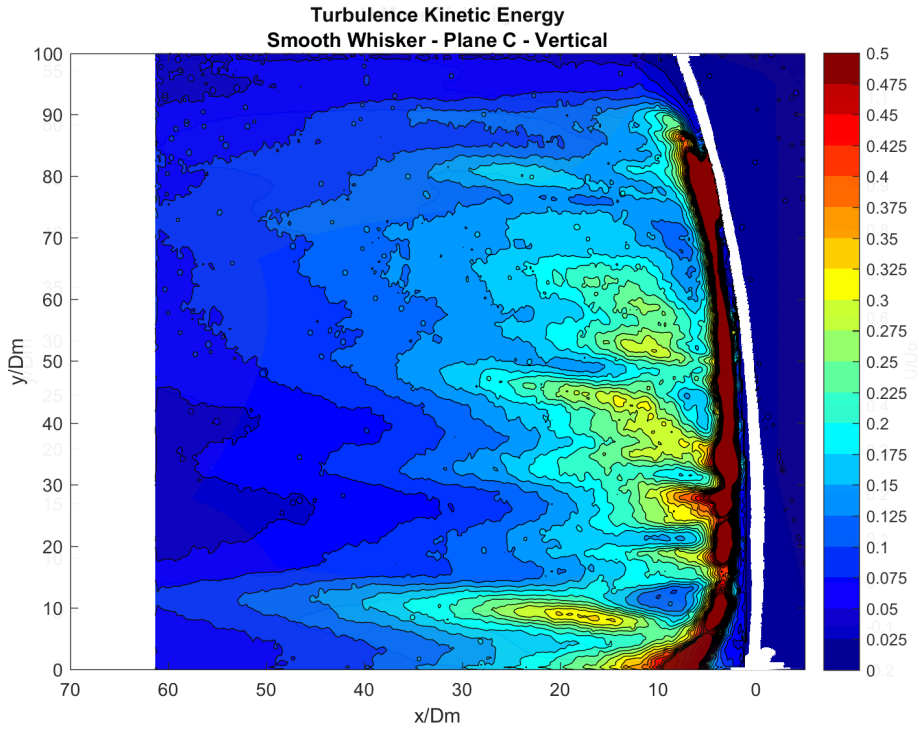

(a) Re = 134

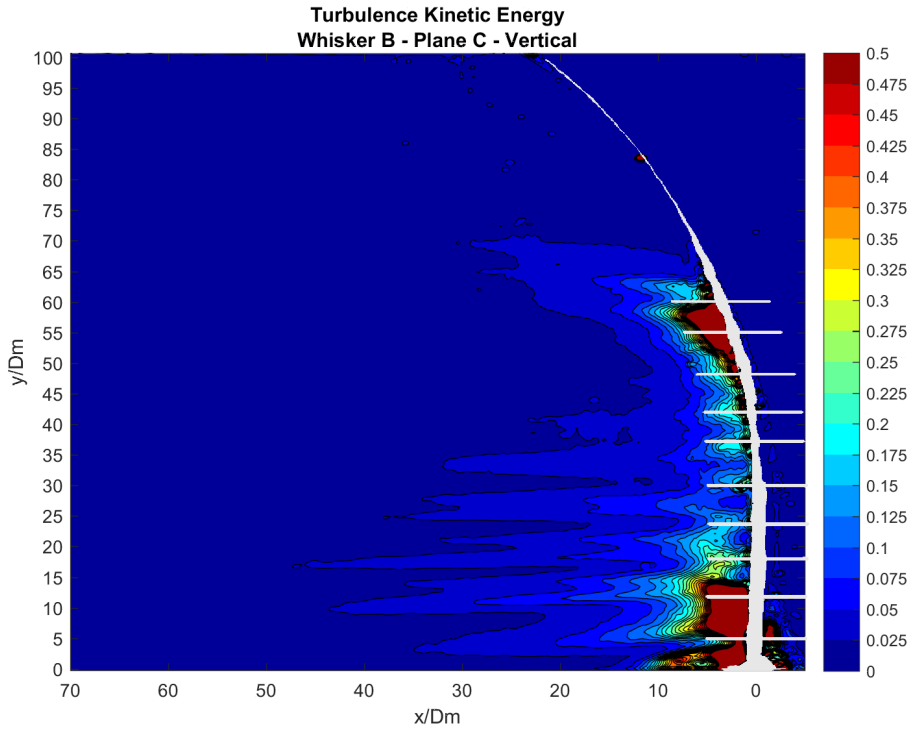

(b) Re = 76

Figure 17: Comparison of the Turbulent Kinetic Energy in the wake of the Smooth Whisker and Whisker B in the vertical plane

extend to 20-30 diameters downstream. Recovery to the freestream turbulence intensity continues beyond the 60 diameters of our field of view. The undulating whisker case has a high turbulence intensity region lasting 10-20 diameters, after which rapid recovery to the mean freestream turbulence occurs.

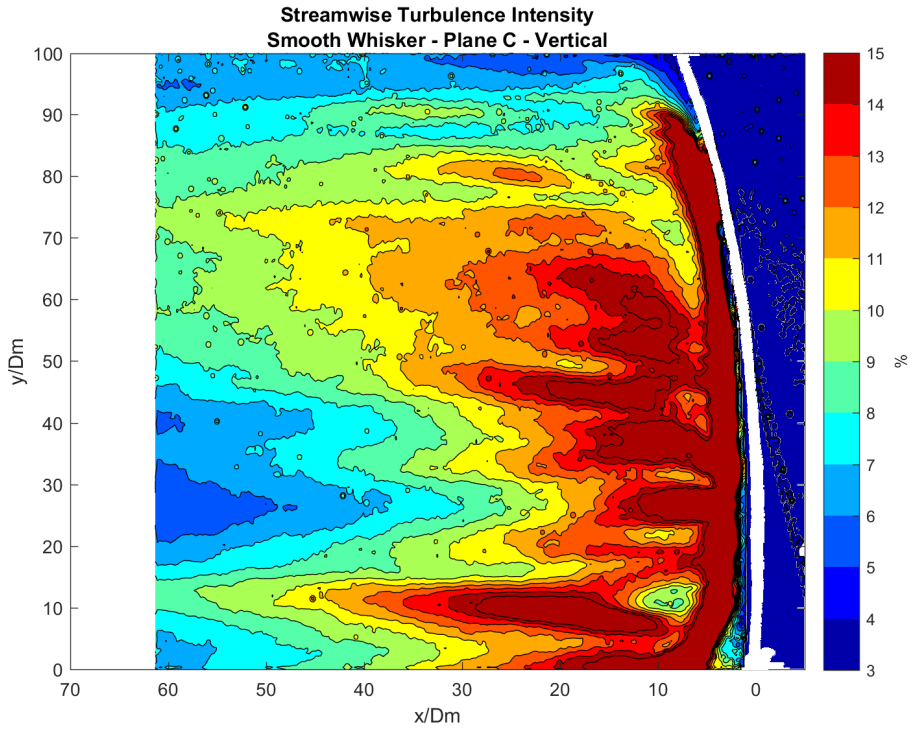

(a) Re = 134

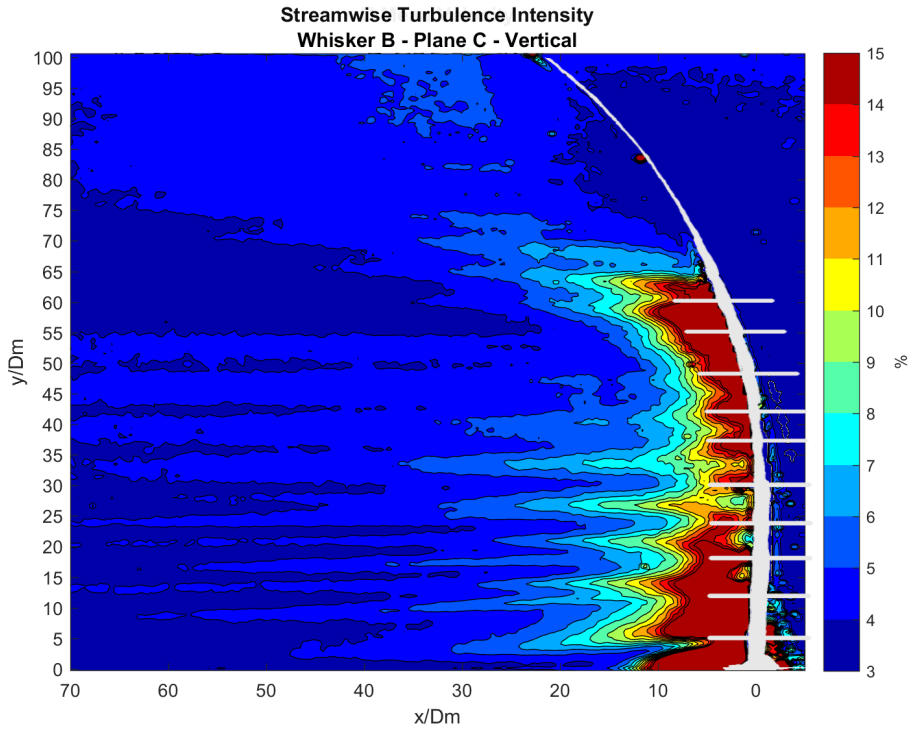

(b) Re = 76

Figure 18: Comparison of the Streamwise Turbulence Intensity in the wake of the Smooth Whisker and Whisker B in the vertical plane

3.1.2 Horizontal Plane

The horizontal plane plots for the wake flow of the smooth whisker and undulating whisker show the difference in the streamwise mean flow pattern of the two cases. As seen in the verical plane in Figure 13a, the smooth whisker case has a very short area of reverse flow followed by a fast recovery to 50 % of the streamwise mean flow. Full flow recovery is much slower and can not be estimated at the distance it occurs in the given plot. The undulating whisker case shows a longer recovery to 50 % of the mean flow compared to the smooth whisker case. However, it begins recovery to the mean flow earlier, following that the undulating whisker cases provide a more predictable wake flow for the streamwise mean velocity. The size of the reverse flow areas also match the results from the vertical plane case.

The W mean plots for the wake flow in Figure 20 share similar wake flow shapes for all three whisker cases. The smooth whisker case shows small amounts of alternating fluctuations downstream similar to the pattern of vortex streets. The undulating whisker's wake flow shows no alternating direction downstream with a longer and slower section of flow returning to the center downstream of the whisker. The wake flow at the peak and trough locations do not significantly vary.

The vorticity plots of the wake flows are compared in Figure 21. The smooth whisker case shows a short area of strong vorticity 4 diameters long. The flow then dissipates to a slightly lower strength, but continues on for the rest of the field of view, showing no sign of recovering. The undulating whisker case show a larger area of strong vorticity. After this strong region, the center plane reduces to very low levels of vorticity while spreading out in a V shaped that continues and slowly reduces quicker than the smooth whisker. This shows the enhanced mixing properties of the whisker are most effective along the center plane, but the vorticity to either side takes longer to dissipate.

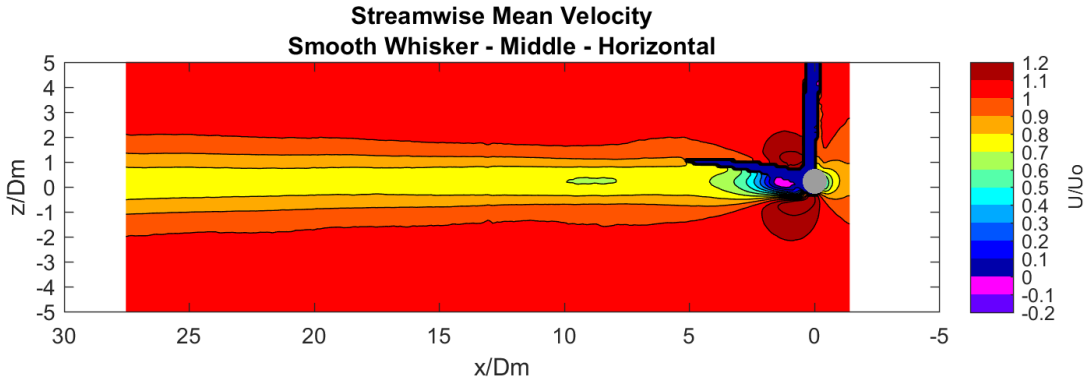

(a) Re = 141

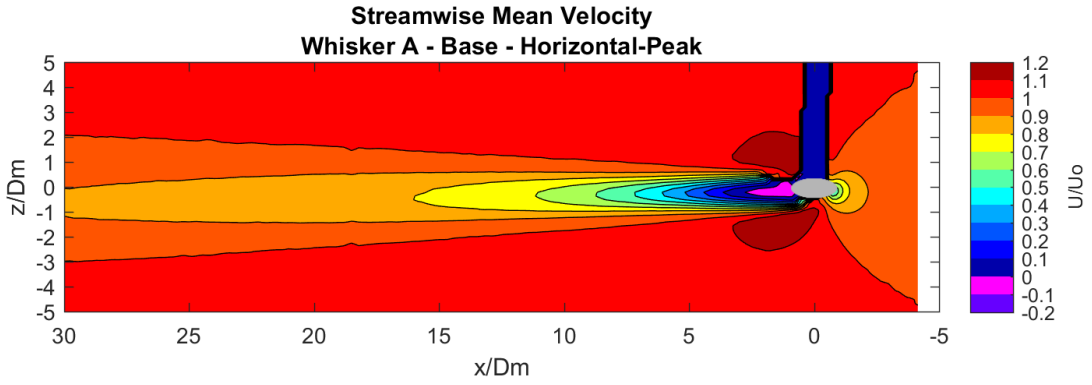

(b) Re = 96

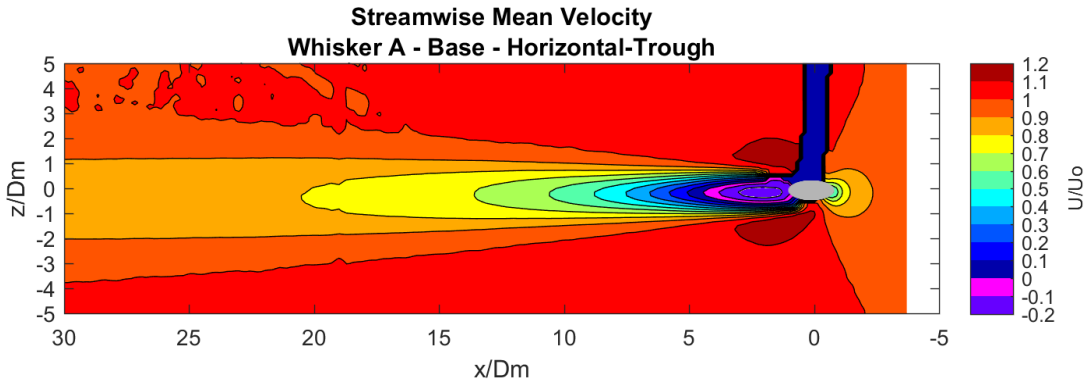

(c) Re = 96

Figure 19: Comparison of the mean streamwise velocity of the wake in a horizontal plane, of the smooth whisker and undulating whiskers (at a peak and trough)

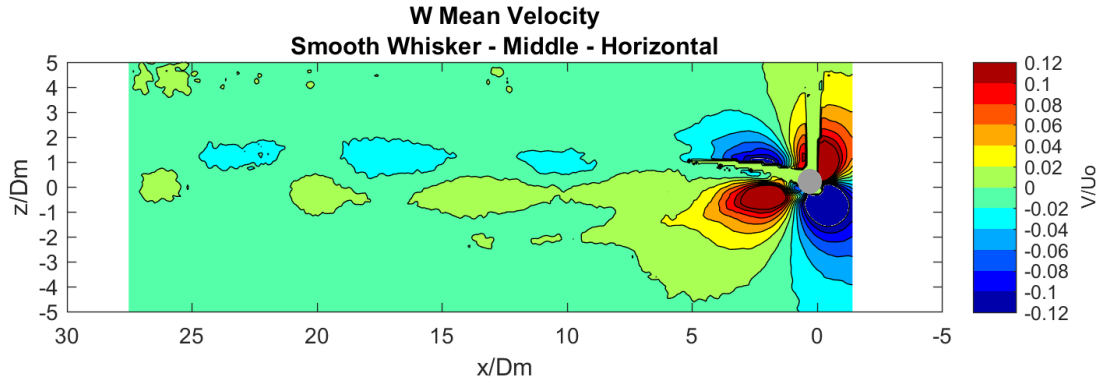

(a) Re = 141

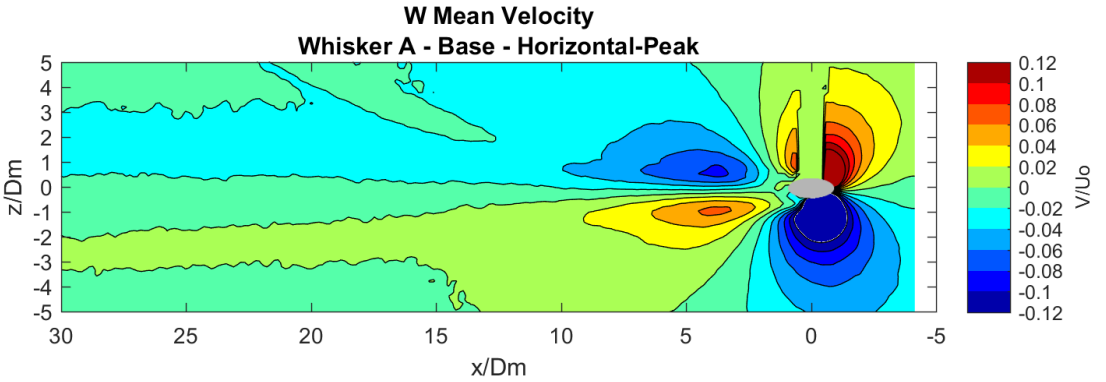

(b) Re = 96

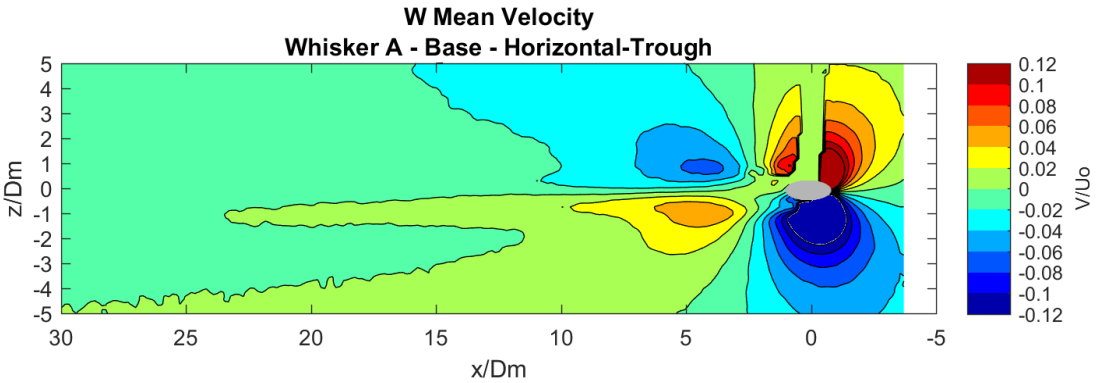

(c) Re = 96

Figure 20: Comparison of the mean vertical velocity of the wake in a horizontal plane, between the smooth whisker and undulating whiskers (at a peak and trough)

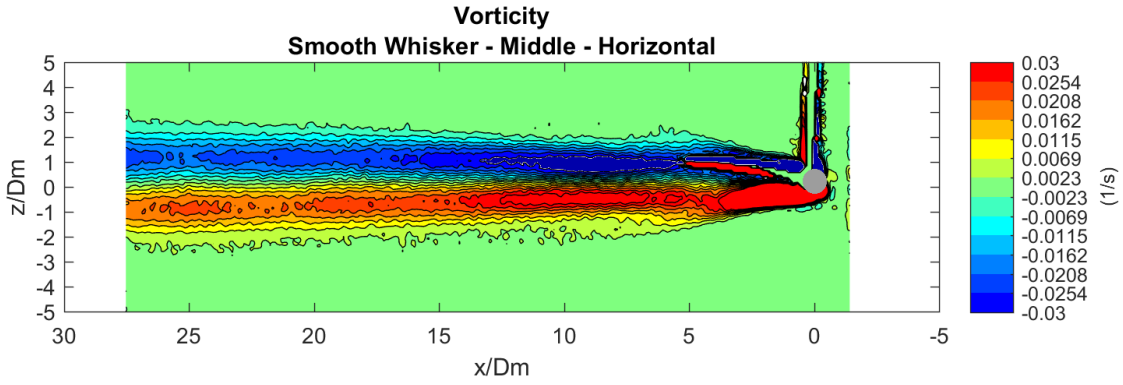

(a) Re = 141

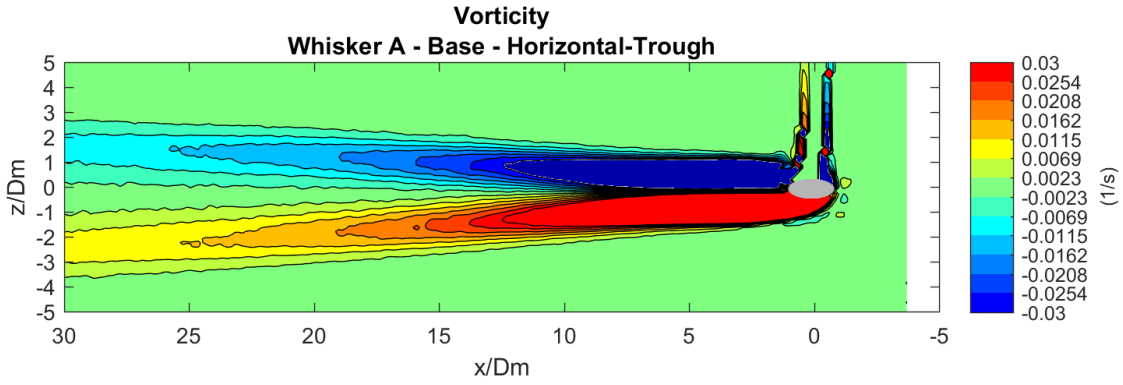

(b) Re = 96

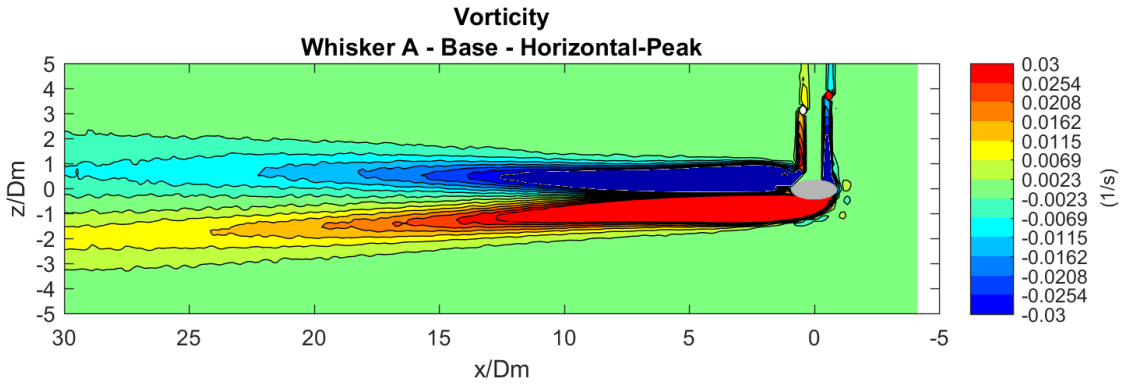

(c) Re = 96

Figure 21: Comparison of the vorticity ω_y in the wake in a horizontal plane, of the smooth whisker and undulating whiskers (at a peak and trough)

The smooth whisker wake flow has a significantly different shape for the Reynolds Shear Stress than the wake flow of the undulating whiskers as shown in Figure 22. A high strength region is seen near the smooth whisker case for 5 diameters, which abruptly changes into a much weaker and slightly prolonged section. There is also shift in sign value at 10 diameters with equal and opposite strengths maintained until fully dissipated. The undulating whisker case show a much different shape. The Reynold stress is strongest 3-5 diameters after the whisker. This strong section is 5 diameters long, which then progressively dissipates out, much like the vorticity strengths. The strength is equal and opposite, with no alternations as seen in the smooth whisker.

The Turbulence Kinetic Energy plots of the wake flow are of interest due to the variances between all whiskers shown in Figure 23. The smooth whisker case shows very high energy levels up to 20 diameters downstream, before beginning to reduce. The wake flow of the undulating whisker shows lower levels of turbulence kinetic energy in the peak plane than in the trough plane by a significant margin. The trough location shows a longer and wider wake as seen in the streamwise mean velocity. Both planes present a gap of 3-5 diameters between the higher energy level sections and the whisker.

The variations in turbulence intensity of the wake flow are compared in Figure 24. The smooth whisker case creates a large area of high turbulence intensity. The high turbulence area lasts for 5 diameters. The outer section remains strong with the center at an intermediate strength. The intensity begins to slowly reduce after 10 diameters, but remains higher than the mean flow for the entire field of view. The turbulence intensity of the wake for the undulating whiskers follow the V shape as seen in the vorticity and Reynolds stress plots. The turbulence intensity starts low and grows to its strongest region 3-5 diameters from the whisker, which is consistent

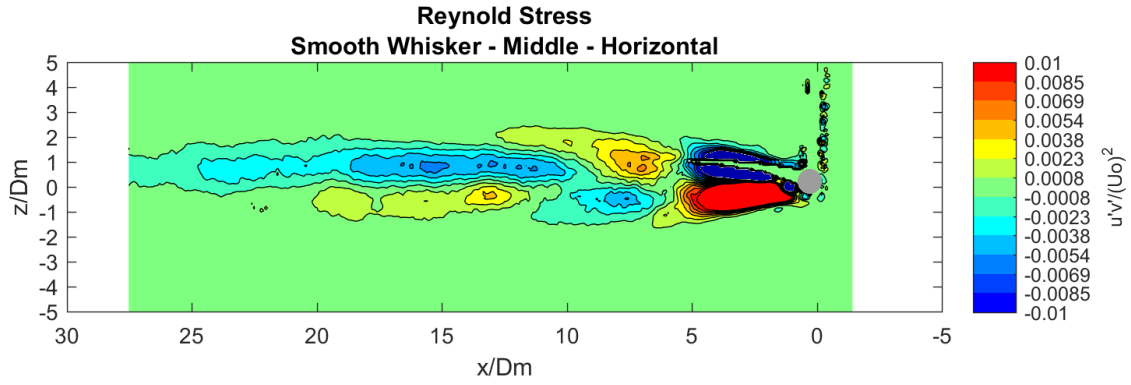

(a) Re = 141

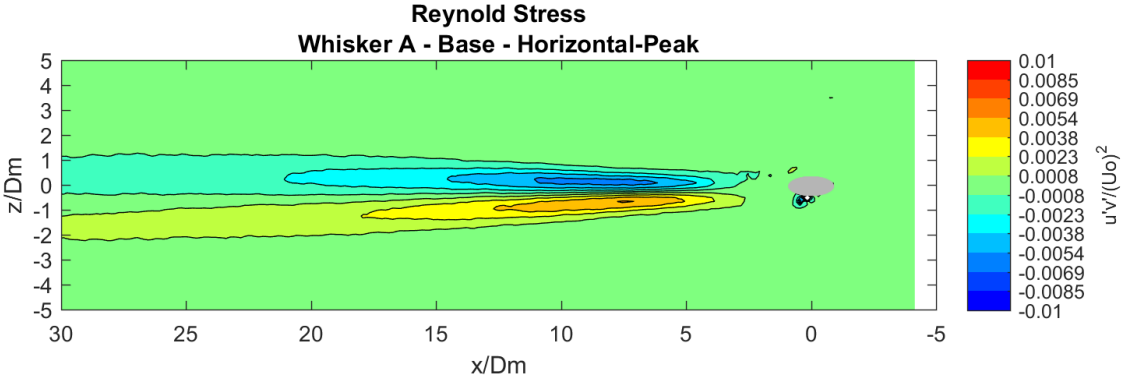

(b) Re = 96

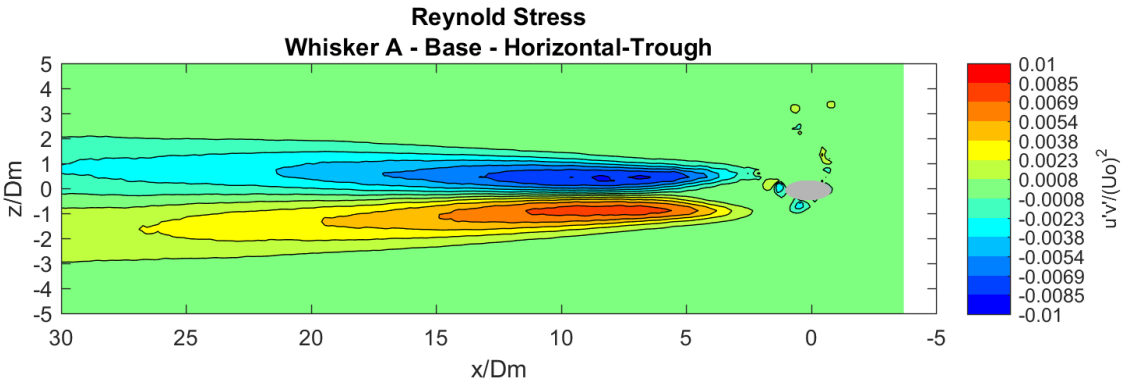

(c) Re = 96

Figure 22: Comparison of the Reynolds shear stress of the wake in a horizontal plane, of the smooth whisker and undulating whiskers (at a peak and trough)

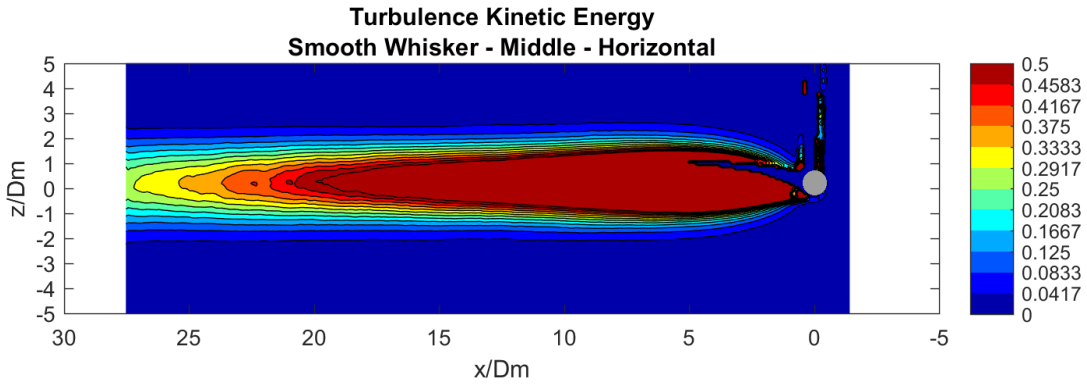

(a) Re = 141

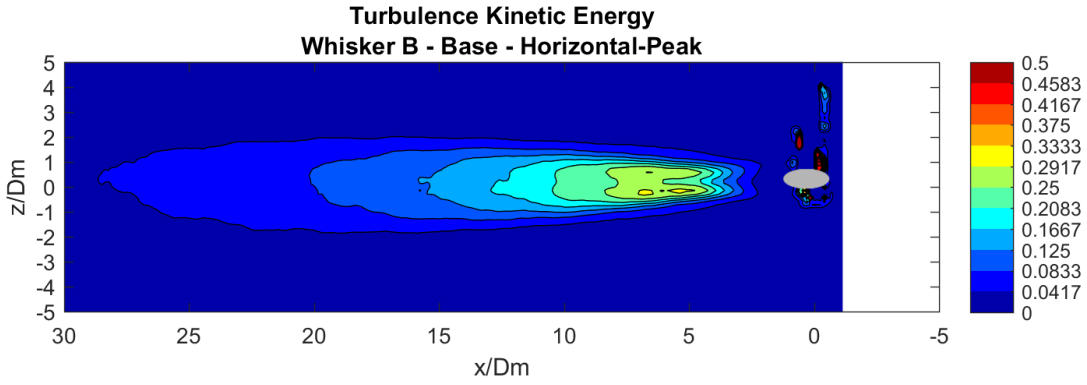

(b) Re = 87

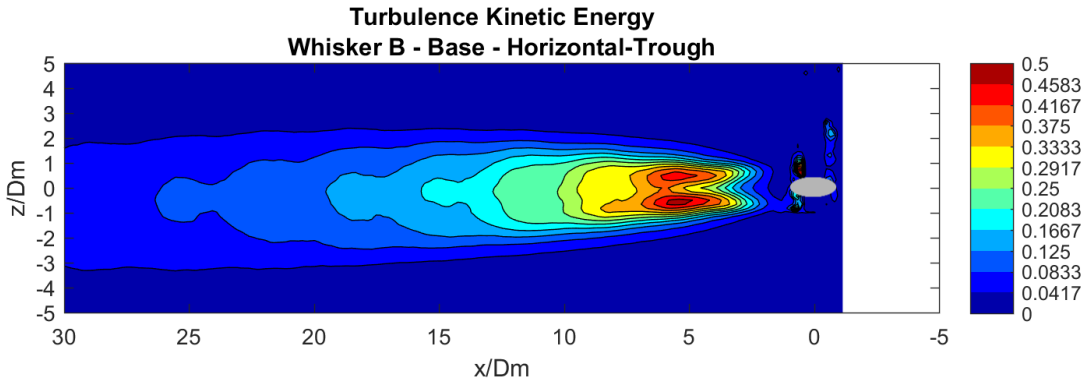

(c) Re = 99

Figure 23: Comparison of the turbulent kinetic energy (T.K.E.) of the wake in a horizontal plane, of the smooth whisker and undulating whiskers (at a peak and trough)

with what is seen in the Reynolds stress and TKE plots.

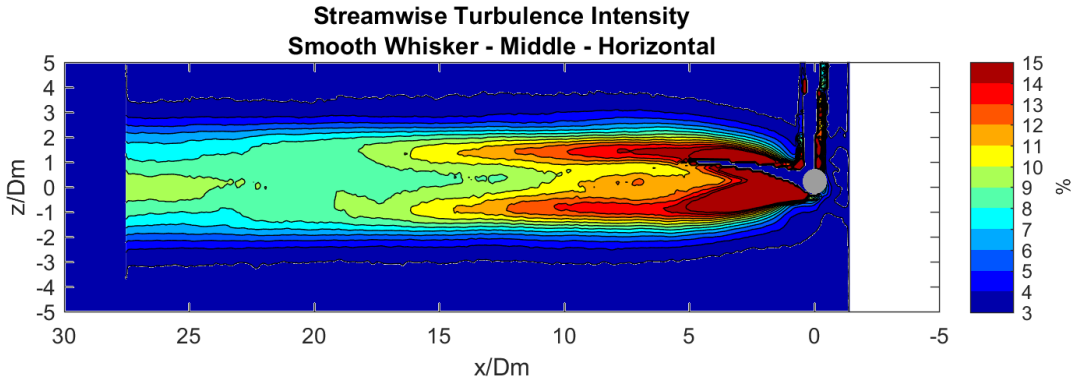

(a) Re = 141

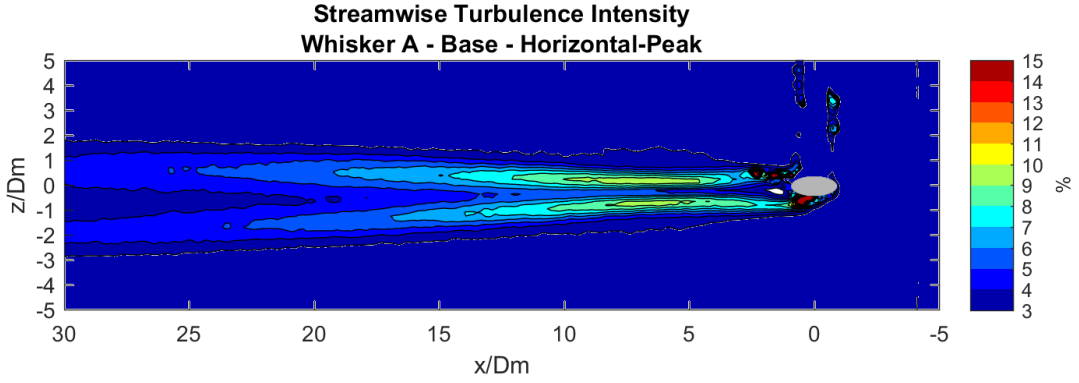

(b) Re = 96

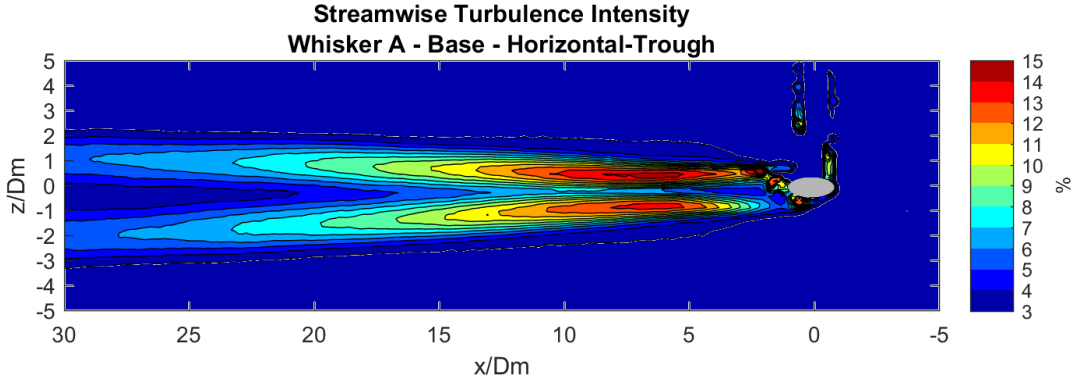

(c) Re = 96

Figure 24: Comparison of the streamwise turbulence intensity of the wake in a horizontal plane, of the smooth whisker and undulating whiskers (at a peak and trough)

3.2 Variations in the Wakes of Whisker Peaks vs Whisker Troughs

The wake structure of the undulating whiskers are compared at the peak and trough locations in the horizontal plane for variations in the wake flow. Figure 25 compares the streamwise mean velocity of the wake at peak and trough locations. The plots show good correlation with the results from the vertical streamwise mean velocity plot in Figure 13b. The peak locations show noticeably lower amounts of reverse flow and a narrower wake in the downstream flow as well as slightly faster flow recovery. The troughs show larger areas of reverse flow and a wake that is a diameter wider than those found at peak locations. These results are consistent for both undulating whiskers at all peak and trough locations.

Figure 26 shows uniformity in the vorticity at different peak and trough locations. Similar strength vortices extend to 15 diameters before gradually weakening. A gap in the centerline is visible starting at 8 diameters. The width of the vortex is also consistent at 5 diameters. The vortices are stronger in the horizontal plane than in the vertical plane as shown in Figure 15b.

There is a significant difference in the turbulence intensity wake flow between peak and trough locations as shown in Figure 27. The maximum turbulence intensity in the base plane is seen to range from 9 % to 22 %. The base trough planes show higher levels of turbulence than the adjacent peak locations. The differences may be due to the geometry variations and differing α and β angles. The gap between the whisker and highest turbulence intensity region varies from 3-5 diameters. The width of the wake in the downstream flow also varies between each plot, ranging from 3-6 diameters. The recovery distance varies significantly, and is not shown to correlate with the peak strength of the turbulence intensity.

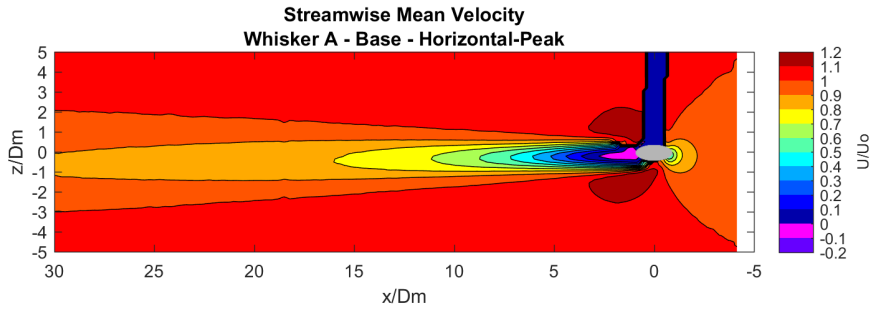

(a) Re = 96

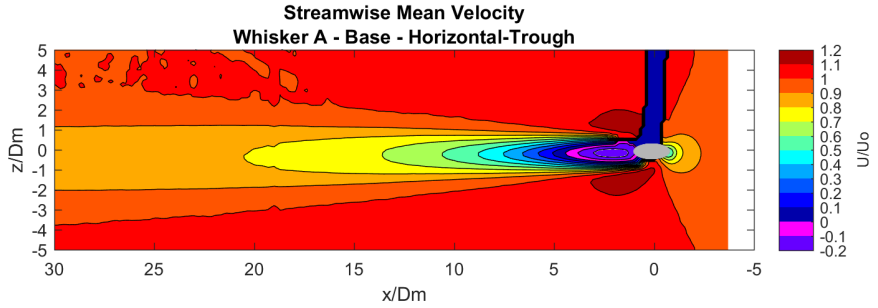

(b) Re = 96

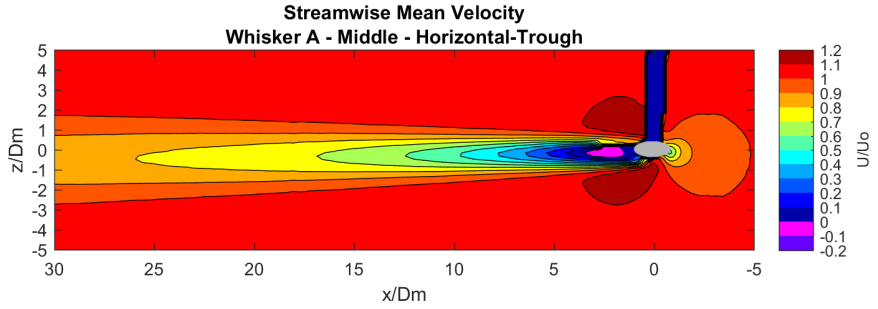

(c) Re = 87

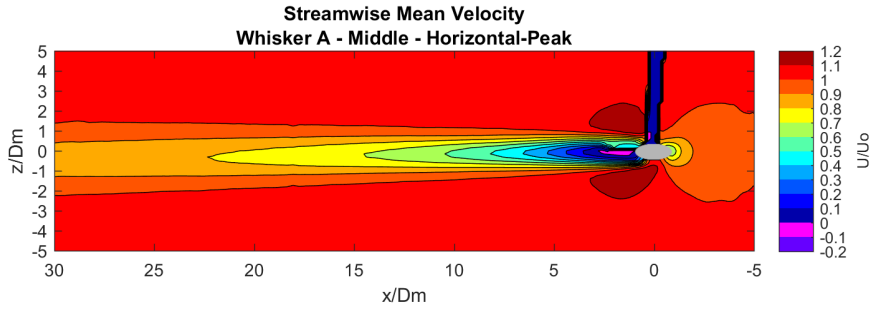

(d) Re = 99

Figure 25: Comparison of the Streamwise Mean velocity in the wake of different peak and trough locations on Whisker A

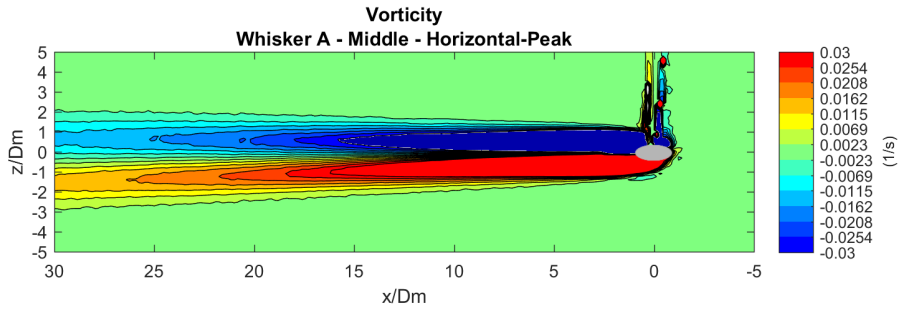

(a) Re = 89

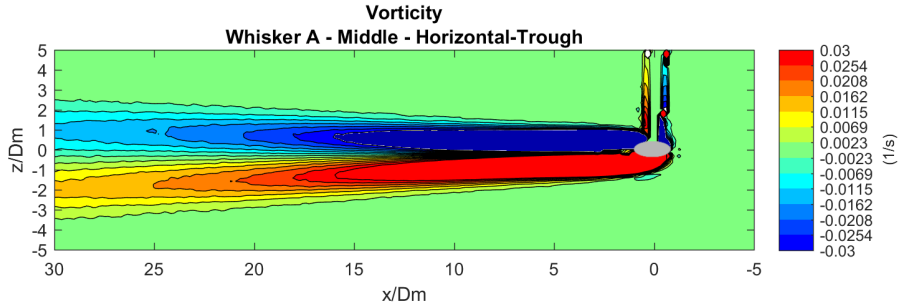

(b) Re = 88

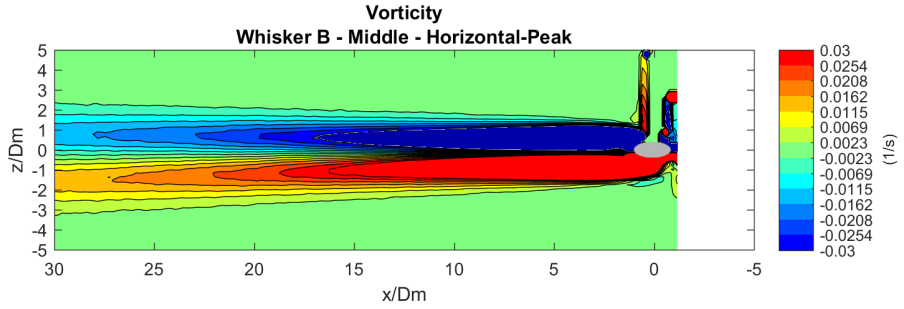

(c) Re = 71

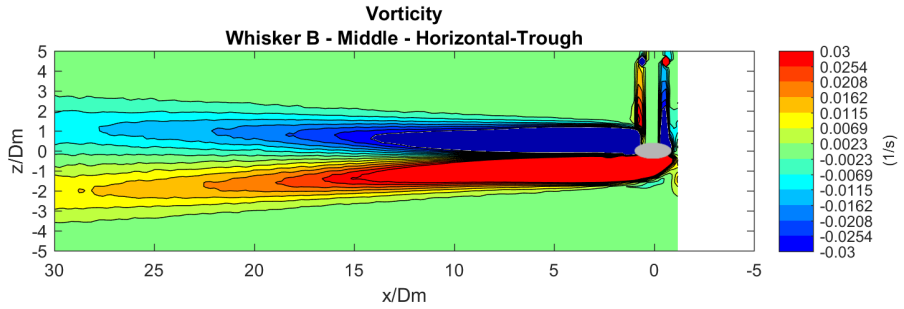

(d) Re = 70

Figure 26: Comparison of the Vorticity in the wake of different peak and trough locations on Whisker A and B

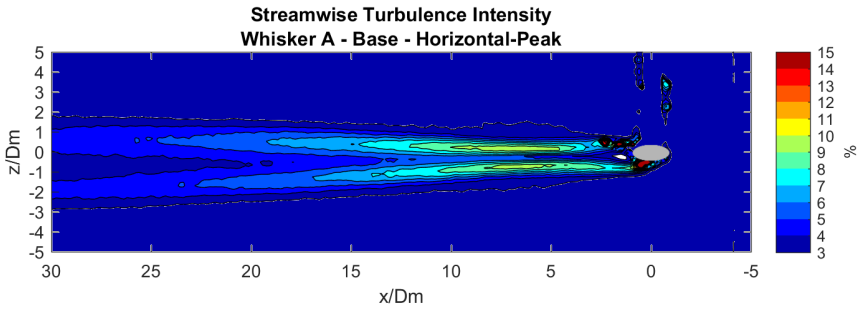

(a) Re = 96

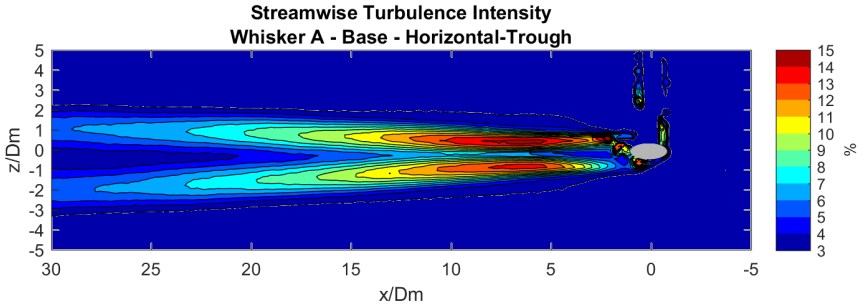

(b) Re = 96

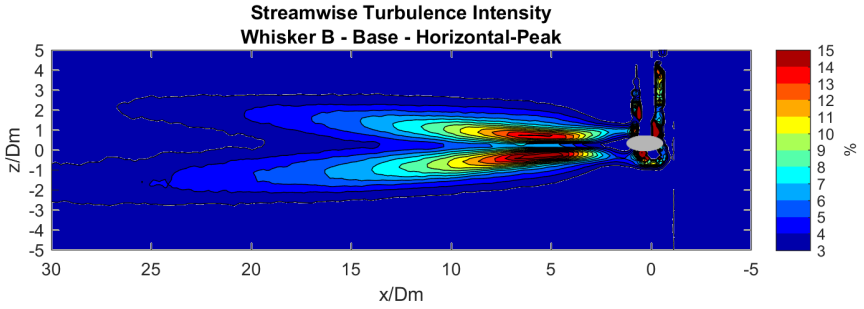

(c) Re = 87

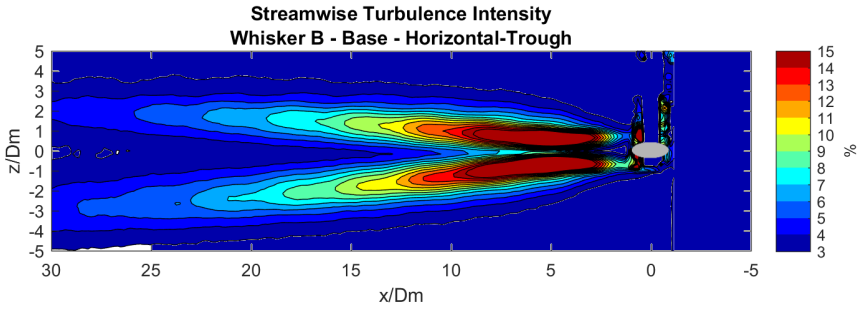

(d) Re = 99

Figure 27: Comparison of the Streamwise Turbulence Intensity in the wake of different peak and trough locations on Whisker A and B

3.3 Wake Structure Comparison to Previous Scaled Undulating Whisker Study

Rinehart performed a study focusing on the effect of the α and β angles on the wake structure of scaled whisker models. Four scaled whiskers were 3D printed and tested in a water channel at Re=630 using 2D PIV. The angle of incidence on the four models were: $\alpha = \beta = 0°$, $\alpha = \beta = -5°$, $\alpha = 5°$ $\beta = -5°$, $\alpha = \beta = -15°$. The study of the angle variations provide insight to some of the possible flow fluctuations of the wake which may occur with the wake in real whiskers as seen in the results for streamwise mean velocity in Figure 28. Since it was not possible to determine the α and β values for the real whiskers due to the limited image resolution, only the $\alpha = \beta = 0°$ results will be used for comparison. Color scales, field of view, and flow direction are matched to Rineharts results, with flow moving from left to right.

Figure 29 compares the streamwise mean velocity and the streamwise turbulence intensity of the wake flow for this study and Rineharts study. For the streamwise mean velocity in the vertical plane, several features match between the two studies. Both plots show the faster recovery sections at the peaks and the slower recovery sections in the trough. The trough locations show larger areas of reverse flow than the peak locations. The results show differences which may be due to the significantly lower Reynolds number. The flow is nearly recovered by 10 diameters in Rineharts results compared to 0.7 75 % for this studys results. The reverse flow areas are also 2 diameters shorter with less definition between peaks and troughs in Rineharts results.

The turbulence intensity plots of the wake flow show similar plots with regard to strength and shape in Figure 29. Neither test case shows strong correlation to the peak and trough locations. The results from Rinehart show higher turbulence levels likely due to the higher Reynolds number.

The vorticity plots in Figure 30 show both cases have pairs of equal and opposite vortices in each trough. The strong vorticy area lasts 4-6 diameters before breaking down to long streaks of low intensity levels.

Good correlation is seen in Figure 31 for the streamwise mean velocity wake flow. Greater reverse flow occurs in the trough locations with faster recovery to the mean flow present in the peak locations. The difference in reynolds numbers appear to only affect the distance required for the flow to recover.

The streamwise turbulence intensity plots in Figure 32 show agreement in shape as well. The intensity in the high turbulence region is much shorter at 1 diameter in Rineharts results vs the 3-5 diameters in this studies results. Both plots show higher turbulence levels in the troughs compared to the peaks.

The results of this comparison show good correlation between the wakes of a scaled model of an undulating whisker to a real undulating whisker. Differences in the wake of the model and real whisker can be attributed to the significant difference in Reynolds numbers. Even with this difference, the defining features of the wakes are clearly present, suggesting that a study comparing a scaled model and a real whisker would show near identical results in the wake structures produced.

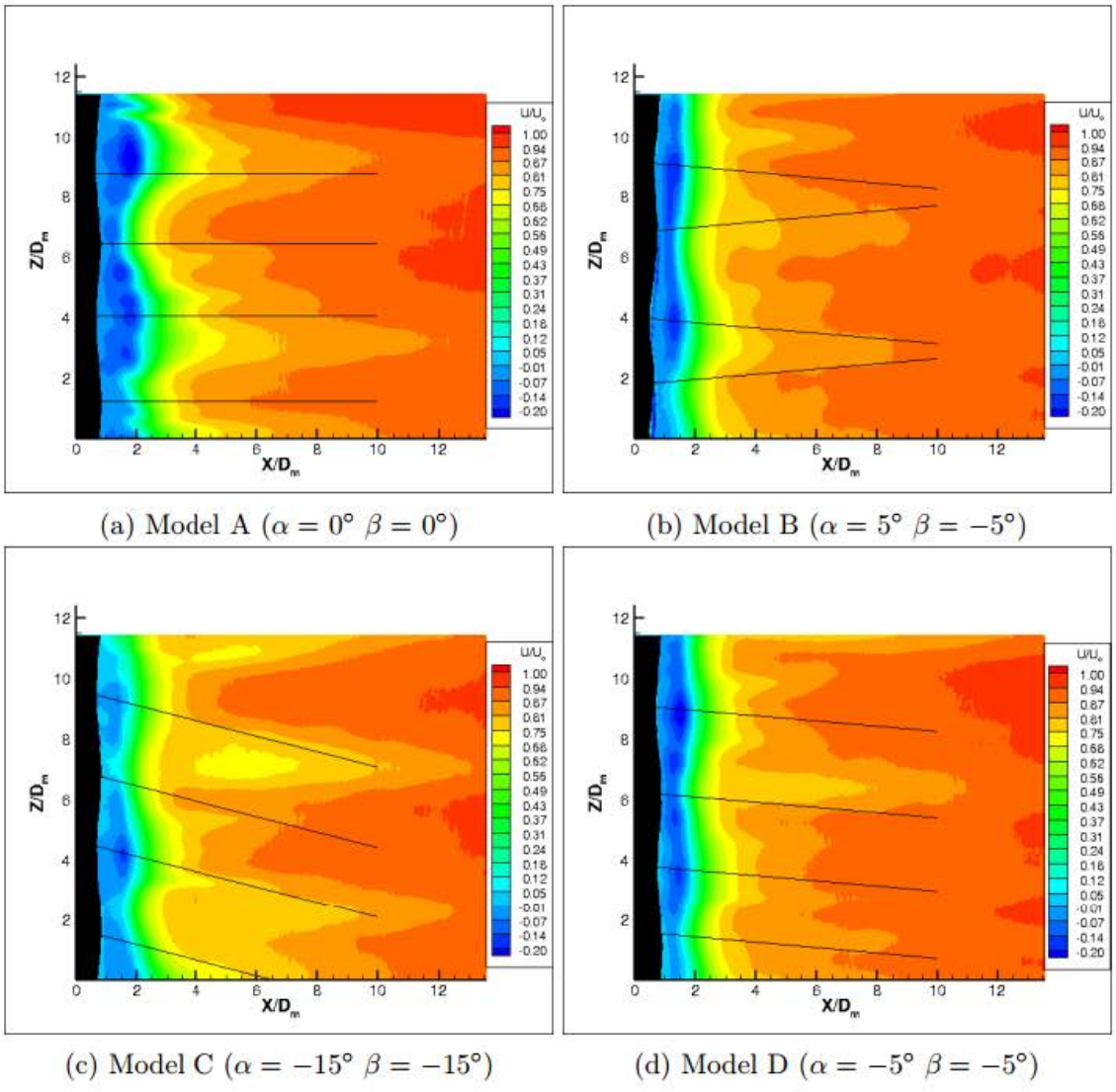

(a) Model A ($\alpha = 0° \ \beta = 0°$)

(b) Model B ($\alpha = 5° \ \beta = -5°$)

(c) Model C ($\alpha = -15° \ \beta = -15°$)

(d) Model D ($\alpha = -5° \ \beta = -5°$)

Figure 28: Streamwise Mean velocity results for four test cases of variations of α and β angles by Rinehart [5]

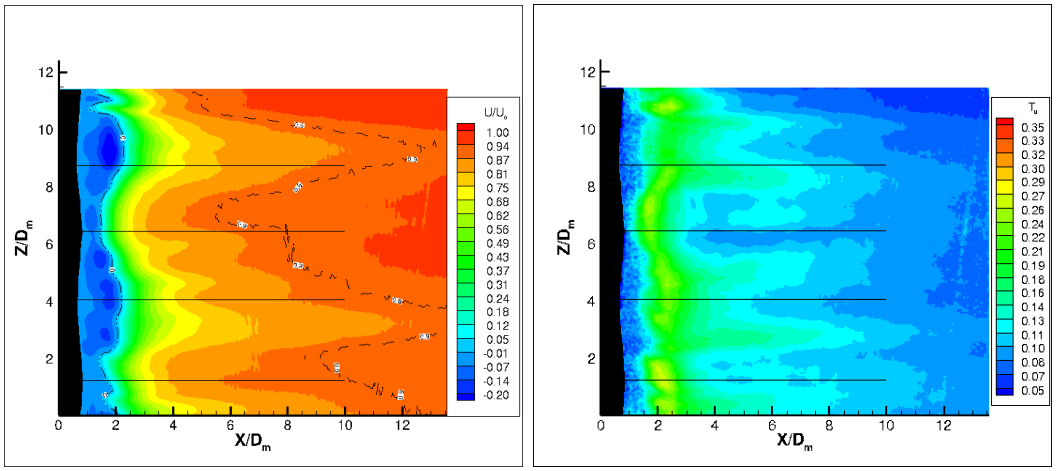

(a) Re = 630 (b) Re = 630

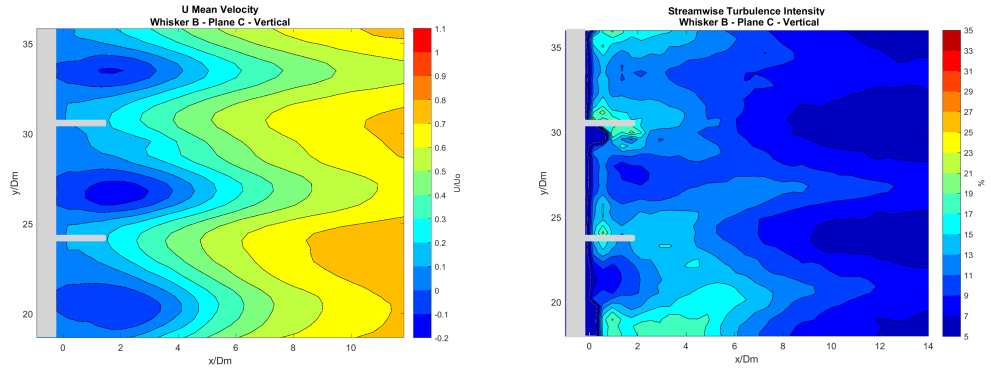

(c) Re = 76 (d) Re = 76

Figure 29: Comparison of the vertical plane plots for streamwise mean velocity and turbulence in the wake for (a) and (b) Rinehart [5] results for $\alpha = \beta = 0$ vs Bunjevac results at (c) and (d) equivalent field of view

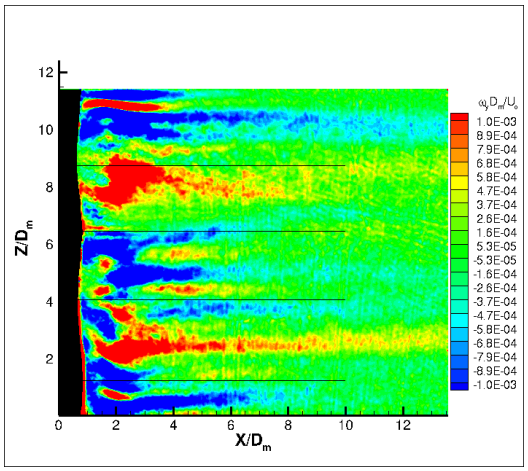

(a) Re = 630

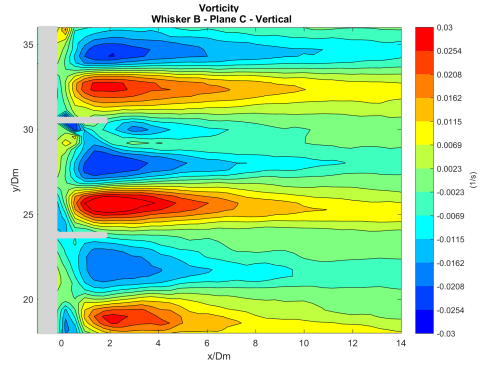

(b) Re = 76

Figure 30: Comparison of the vertical plane plots for vorticity in the wake for Rinehart [5] results vs Bunjevac results

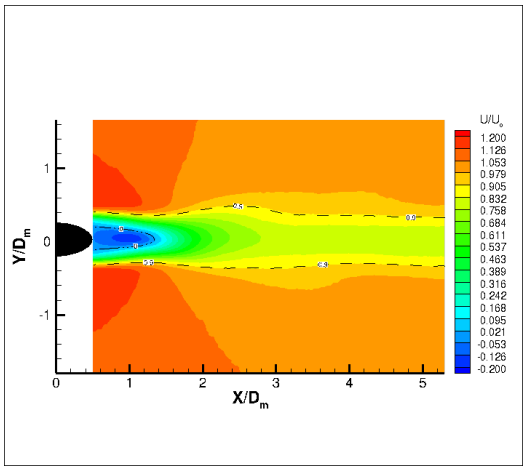

(a) Re = 630

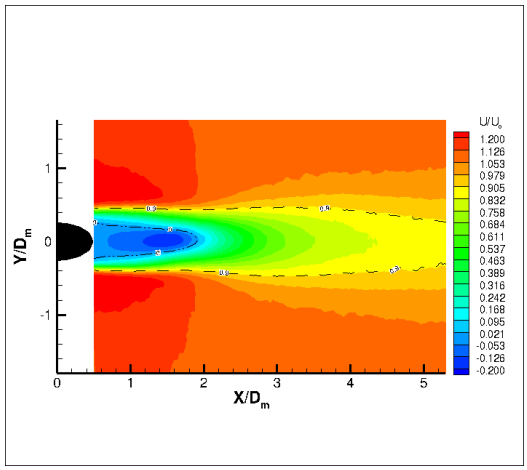

(b) Re = 630

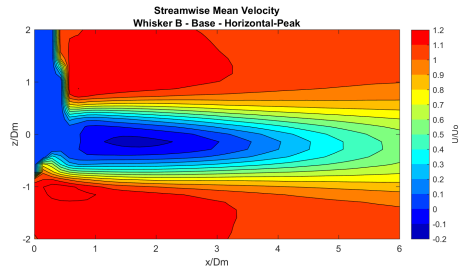

(c) Re = 76

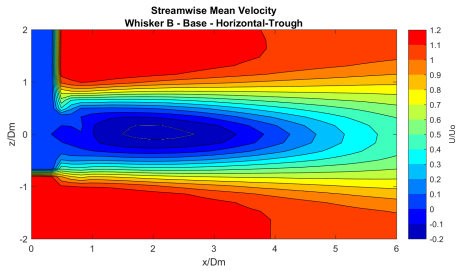

(d) Re = 76

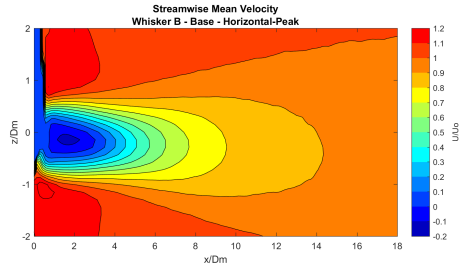

(e) Re = 76

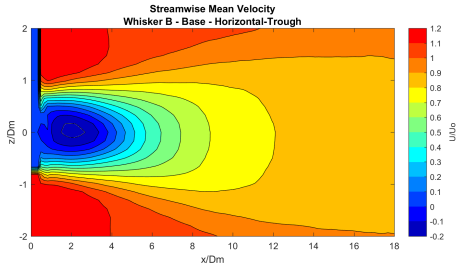

(f) Re = 76

Figure 31: Comparison of the horizontal plane plots for streamwise mean velocity in the wake of (a) and (b) Rinehart [5] results for $\alpha = \beta = 0$, Bunjevac results at (c) and (d) at equivalent field of view, and (e) and (f) Bunjevac results at longer field of view

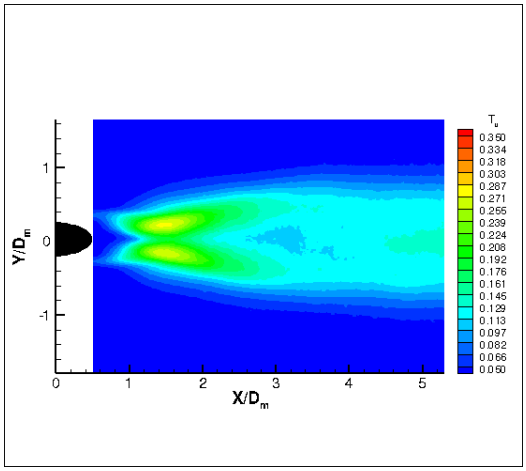

(a) Re = 630

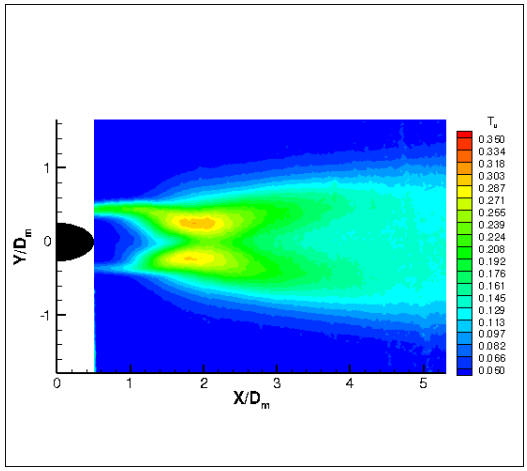

(b) Re = 630

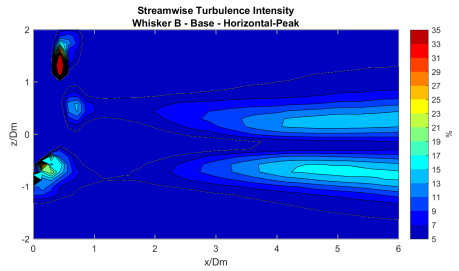

(c) Re = 76

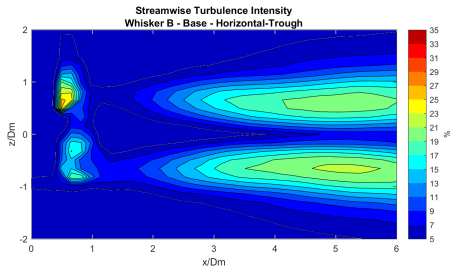

(d) Re = 76

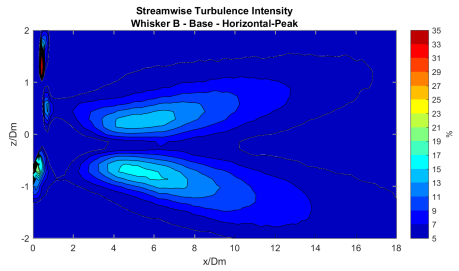

(e) Re = 76

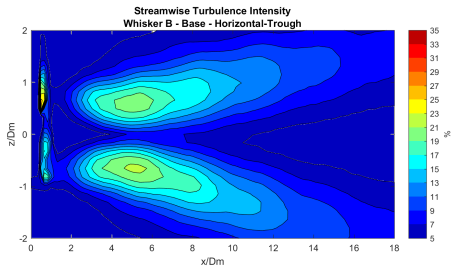

(f) Re = 76

Figure 32: Comparison of the horizontal plane plots for streamwise mean turbulence in the wake of (a) and (b) Rinehart [5] results for $\alpha = \beta = 0$, Bunjevac results at (c) and (d) at equivalent field of view, and (e) and (f) Bunjevac results at longer field of view

3.4 Flow Parameters with a Gap in the Wake Behind Undulating Whiskers

The undulating whisker shapes ability to create a low turbulence intensity region in the wake directly behind the whisker for a significant distance appears to provide the ability to suppress vortex reduced vibration. This gap is visible in the Reynold stress, turbulence intensity, and the streamwise and horizontal RMS plots.

The streamwise turbulence intensity shows a steady growth in strength after the whisker over a distance of 3-5 diameters. The intensity reaches a peak near 15 % in the case of Figure 33a, but has reached 25 % in other results as seen in Figure 27d. The higher intensity region, which we define as the upper third portion of the value scale, lasts for nearly 5 diameters over the 20-35 diameter area which the turbulence intensity is several percent above the mean turbulence intensity.

Figures 33b and 33c show the reynolds stress and the RMS values for the streamwise velocities have a very similar growth and decay pattern as the turbulence intensity. The distance between the highest strength region and the whisker is at 3-5 diameters and the size of the higher intensity region is also near 5 diameters long.

Figures 33e shows the horizontal rms values. The higher intensity region is slightly further away than the streamwise turbulence intensity region at 7 diameters. The strength is approximately 33 % lower than in the streamwise direction.

The undulating whiskers shape creates very strong and consistent vorticities as showin in Figure 33d. They appear to be strong enough that the opposing vortices do not mix or interact with each other until further downstream. Rather than creating alternating vortexes as a blunt body or cylinder would, the undulating shape creates simultaneous pairs of streamwise vortices. With equal forces on each side of the whisker, the amount of force induced on the whisker is minimized.

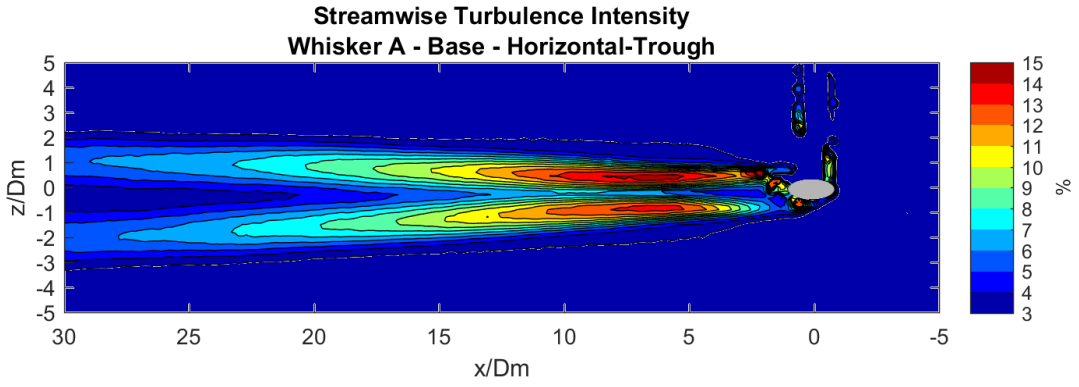

(a) Re = 96

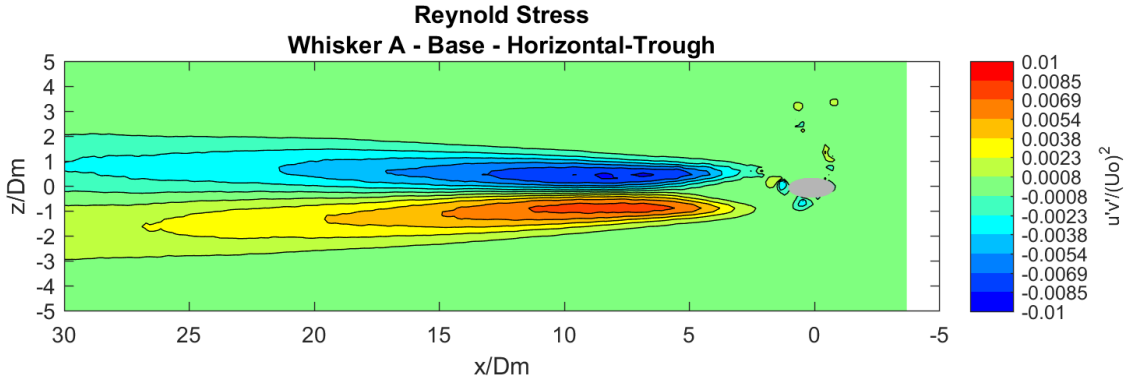

(b) Re = 96

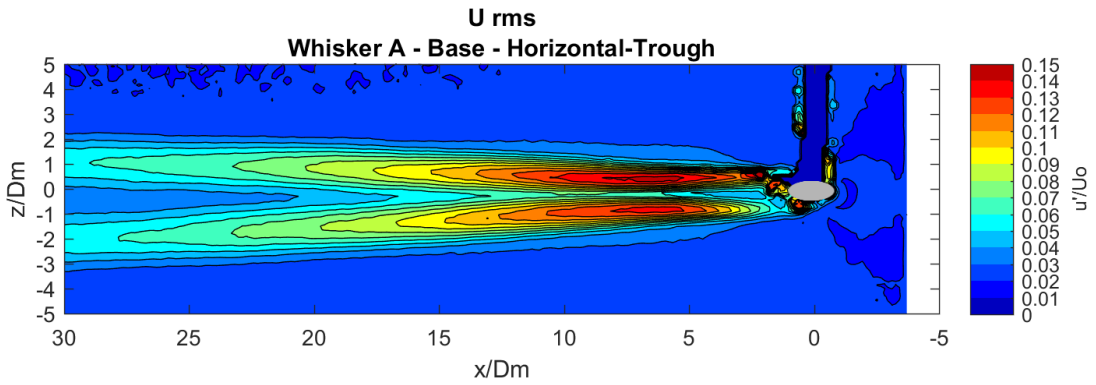

(c) Re = 96

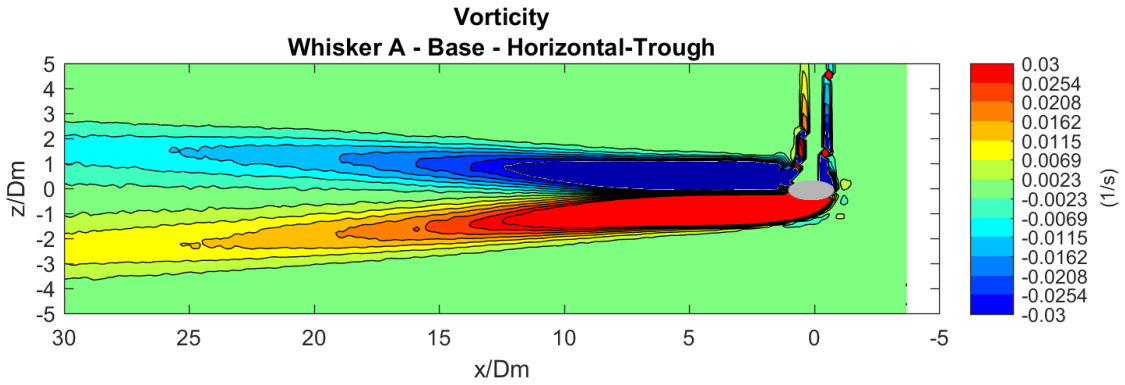

(d) Re = 96

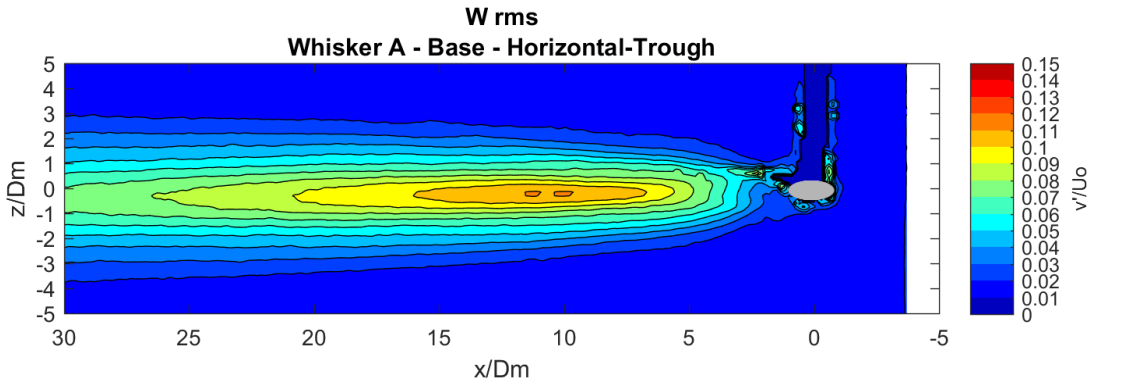

(e) Re = 96

Figure 33: Horizontal plane data analyzing the features of the low turbulence gap of the wake for multiple flow parameters

CHAPTER IV

Conclusions

The goal of this study was to provide details on the wake flow of real undulating seal whiskers at low reynolds numbers and determine the key flow features which provide undulating whiskers their Vortex Induced Vibration supression abilities. The Reynolds numbers for the experiment ranged from 62 to 156. Undulating whiskers are able to produce a wake flow with a predictable flow structure when compared to the wakes of smooth cylindrical whiskers. The strong vorticy mixing predicted by previous studies [1] is induced by the two plane undulations which result in the peak and trough geometries. This geometry minimized the turbulence directly behind the whisker, resulting in minimal vortex induced vibrations.

The undulations of the whiskers provide a predictable streamwise mean flow pattern. The flow velocities at the peak and trough location are clearly distinct from each other. The wake flow at the thinner, longer peak locations on undulating whiskers consistently have lower amounts of reverse flow and a faster recovery. The wake flow at the wider, shorter troughs have larger reverse flow areas and a longer recovery. This difference is significant enough that horizontal plane data can be clearly

identified by observing the reverse flow region and the width of the wake flow.

The vorticity plots show equal and opposite pairings in both the vertical and horizontal plots as described by Lins [2] work with wavy cylinders. The vertical plane shows that traces of the vortices can linger for a significant distance, while the horizontal plane shows the fast dissipation along the centerline.

The Turbulence Kinetic Energy, Reynold Stress, and Streamline Turbulence Intensity plots show the flow features which are produced in the flow by the undulating whiskers, giving their ability to suppress vortex induced vibrations. In each plot, an area of low intensity is clearly visible between the whisker and the start of the strongest area of intensity. This gap is typically 3-5 diameters long at low Reynolds numbers, which appears to be far enough away to not affect the whisker. The strength of the vorticity may provide sufficiently smooth flow to prevent major flow fluctuations near the whisker.

The general shape of the wake geometry for the undulating whiskers aligns with the results provided in Rineharts [5] idealized whisker study for the 0° case. The study shows the alignment of the faster recovering sections with the peaks at zero angle of incidence. Vorticity pairing is clearly seen between peaks and troughs and matches well between the two test cases in the size of the flow features downstream of the whiskers. Critically, the gap from the whisker to the strong turbulence intensity region is present in Rineharts scaled model case. Part of the reason for the smaller gap distance in the idealized case may be the higher Reynolds number of 630. The major shifting of features due to the variations of angle of incidence is not clearly seen in the real whisker data, although this was not a focus of this study.

CHAPTER V

Future Work

The findings from this study have shown many interesting flow characteristics that warrant future study. There are a few key areas that should be addressed to expand upon the provided information. Testing real whiskers at multiple Reynolds numbers would allow better comparison to previous studies. The highest Reynolds number in this experiment was 152, which is significantly lower than other studies which used a Reynolds number ranging from 600 to 3000. The Reynolds numbers experienced by real Elephant Seals is in the range of Controlling the Reynolds number would allow better comparisons of different peaks and troughs at different positions along the whisker.

Since the flow is highly three dimensional, 3D Tomographic PIV would provide a more complete picture of the real flow around the whiskers. Only a 2D PIV system was available for use for this study, limiting the information which could be collected. This especially limited data in the vertical plane, as the whisker curved in and out of the lightsheet. Tomographic PIV would allow simultaneous collection of data from all planes, including planes perpendicular to the streamwise flow. This plane

would provide information on the vortex generation as visually described by Lin [2] in Figure 5. Tomographic PIV would also eliminate the difficulty of aligning the vertical lightsheet at the whisker center plane.

Studying different arrays of multiple whiskers would be another interesting experiment. Seals have a multitude of whiskers at various locations. Placing whiskers in tandem would create additional vortices interactions which would be an interesting area to study. Determining if any interactions or optimal placements to maintain a high level of flow sensitivity would be helpful for future sensor development.

Validation of Rineharts study of flow modification using α and β could also be of interest. Determining if any shifting of flow structures occurs would be verification of those results, although matching angles of incidence from the study with those on real whiskers would be difficult due to the random variations of angles of incidence of real whiskers.

BIBLIOGRAPHY

[1] W. Hanke, M. Witte, L.I. Miersch, M. Grede, J. Oeffner, M., Michael, F. Hanke, A. Leader, G. Denhardt, "Harbor Seal Vibrissae Morphology Suppresses Vortex-Induced Vibrations," *The Journal of Experimental Biology* volume 213, pp.2665-2672 2010.

[2] Y.F. Lin, H.L. Bai, Md. Mahbub Alam, W.G. Zhang, K. Lam, "Effects of large spanwise wavelength on the wake of sinusoidal wavy cylinder", *Journal of Fluids and Structures*, volume 61, pp. 392-409 2016.

[3] J.H. Jung, H.S. Yoon, "Large Eddy Simulation of Flow Over a Twisted Cylinder at a Subcritical Reynolds Number", *Journal of Fluid Mechanics*, volume 759, pp. 579-611 2014.

[4] W. Zhang, Dainchin S.J. Lee "PIV Measurements of the Near-Wake Behind a Sinusoidal Cylinder", *Experiments in Fluids*, volume 38, pp. 824-832 2005.

[5] A. Rinehart, W. Zhang A Characterization of Seal Whisker Morphology and the Effect of Angle of Incidence of Wake Structures, Masters Thesis Dissertation, Cleveland State University, 2016.

[6] C. Ginter, T. DeWitt, F. Fish, C. Marshall, "Fused Traditional and Geometric Morphometerics Demonstrate Pinniped Whisker Diversity" PLoS ONE volume 7 issue 4 2012.

[7] J. E., King, Seals of the World, Ithaca: Cornell University Press 1983.

[8] J. K., Ling, "Vibrissae of marine mammals", *Functional anatomy of marine mammals*, London: Academic Press, pp. 387-415, 1977.

[9] D. Renouf, Fishing in captive harbour seals. A posible role foe vibrissae. *Netherlands Journal of Zoology*, volume 303 pp. 504-509 1980.

[10] R. Elsner, D. Wartzok, N.B. Sonafrank, B.P. Kelly, "Behavioral and physiological reactions of arctic seals during under-ice pilotage," *Canadian Journal of Zoology*, volume 67, pp. 2506-2513 1989.

[11] H. Hans, J. Miao, M. Triantafyllou, G. Weymouth, "Whisker-like Geometries and Their Force Reduction Properties," *OCEANS MTS/IEEE Conference*, 2013.

[12] H. Beem, "Passive Wake Detection Using Seal Whisker-Inspired Sensing" PhD Dissertation, Joint Program in Oceanography and Applied Ocean Sciences and Engineering, MIT and WHOI, Cambridege, Mass. 2015.

[13] C. Murphy, W. Eberhardt, B. Calhoun, K. Mann, D. Mann, "Effect of Angle on Flow-Induced Vibrations of Pinniped Whisker Diversity," *PLoS ONE*, volume 8, issue 4, 2012.

[14] S. Wang, Y. Liu "Wake dynamics behind a sealvibrissashaped cylinder: a comparative study by timeresolved particle velocimetry measurements" *Experiments in Fluids*, volume 57, 2016.

[15] V. Shyam, A. Ameri, P. Pointsatte, D. Thurman, A. Wroblewski, C. Synder, "Application of Pinniped Vibrissae to Aeropropulsion." *Proceedings of ASE Turbo Expo* 2015.

[16] H. Beem, Y. Liu, G. Barbastathis, M. Triantafyllou "Vortex-induced vibration measurements of seal whiskers using digital holography" *IEEE - OCEANS* 2014.

[17] E. DeArmon, M. Stone, E. Rogenski, D. Thurman, P. Poinsatte, V. Shyam, "Characterization and Analysis of Phoca Vitulina, Zalophus Californianus and

Mirounga Angustirostis Vibrissae", NASA Technical Manual, (pending publication).

[18] M. Witte, W. Hanke, S. Wieskotten, L. Miersch, M. Brede, G. Dehnhardt, A. Leder "On the wake ow dynamics behind harbor seal vibrissae: a uid mechanical explanation for an extraordinary capability" *Nature-inspired uid mechanics* pp. 271-289 2012.

[19] W. Hanke, G. Dehnhardt, "Vibrissal Touch in Pinnipeds" *Scholarpedia of Touch* Volume 10-3 pp. 6828 2015.

[20] H. Hans J.M. Miao, M.S. Triantafyllou "Mechanical characteristics of harbor seal (Phoca vitulina) vibrissae under different circumstances and their implications on its sensing methodology" *Bioinspiration and Biomimetics* Volume 9 036013 2014.

[21] J. Wagner "Karmansche Wirbelstra β e groβe Reynoldszahl" URL:https://upload.wikimedia.org/wikipedia/commons/c/ce/Karmansche_Wirbelstr_groβe_Re.JPG 2014.